The Potato Virus X TGBp2 Movement Protein Associates with Endoplasmic Reticulum-Derived Vesicles during Virus Infection[1]

Ho-Jong Ju, Timmy D. Samuels, Yuh-Shuh Wang, Elison Blancaflor, Mark Payton, Ruchira Mitra[2], Konduru Krishnamurthy[3], Richard S. Nelson, and Jeanmarie Verchot-Lubicz*

Department of Entomology and Plant Pathology (H.-J.J., T.D.S., R.M., K.K., J.V.-L.), and Department of Statistics (M.P.), Oklahoma State University, Stillwater, Oklahoma 74078; and Plant Biology Division, The Samuel Roberts Noble Foundation, Ardmore, Oklahoma 73401 (Y.-S.W., E.B., R.S.N.)

The green fluorescent protein (GFP) gene was fused to the potato virus X (PVX) TGBp2 gene, inserted into either the PVX infectious clone or pRTL2 plasmids, and used to study protein subcellular targeting. In protoplasts and plants inoculated with PVX-GFP:TGBp2 or transfected with pRTL2-GFP:TGBp2, fluorescence was mainly in vesicles and the endoplasmic reticulum (ER). During late stages of virus infection, fluorescence became increasingly cytosolic and nuclear. Protoplasts transfected with PVX-GFP:TGBp2 or pRTL2-GFP:TGBp2 were treated with cycloheximide and the decline of GFP fluorescence was greater in virus-infected protoplasts than in pRTL2-GFP:TGBp2-transfected protoplasts. Thus, protein instability is enhanced in virus-infected protoplasts, which may account for the cytosolic and nuclear fluorescence during late stages of infection. Immunogold labeling and electron microscopy were used to further characterize the GFP:TGBp2-induced vesicles. Label was associated with the ER and vesicles, but not the Golgi apparatus. The TGBp2-induced vesicles appeared to be ER derived. For comparison, plasmids expressing GFP fused to TGBp3 were transfected to protoplasts, bombarded to tobacco leaves, and studied in transgenic leaves. The GFP:TGBp3 proteins were associated mainly with the ER and did not cause obvious changes in the endomembrane architecture, suggesting that the vesicles reported in GFP:TGBp2 studies were induced by the PVX TGBp2 protein. In double-labeling studies using confocal microscopy, fluorescence was associated with actin filaments, but not with Golgi vesicles. We propose a model in which reorganization of the ER and increased protein degradation is linked to plasmodesmata gating.

Plant viruses use the cellular endomembrane system to support virus replication (Schaad et al., 1997; Reichel and Beachy, 1998; Carette et al., 2002a, 2002b; Schwartz et al., 2002). Among positive-strand RNA viruses, the viral replicase is typically anchored to membranes associated with the endoplasmic reticulum (ER), the endocytic pathway, or cellular organelles (Rubino and Russo, 1998; Mas and Beachy, 1999; Rubino et al., 2001; Schwartz et al., 2002, 2004). Many viral replication-associated proteins cause reorganization of cellular membranes with the purpose of creating centers that protect the viral replication complexes (VRCs) from cellular nucleases and host defenses (Schwartz et al., 2002, 2004; Ding et al., 2004). Specifically, the replication complexes of plant viruses belonging to the genera Potyvirus, Comovirus, Dianthovirus, Pecluvirus, and Bromovirus cause proliferation and vesiculation of either the perinuclear or the cortical ER (Schaad et al., 1997; Dunoyer et al., 2002; Lee and Ahlquist, 2003). The replicases of cowpea mosaic virus and red clover necrotic mosaic virus induce ER proliferation (Carette et al., 2002a, 2002b; Turner et al., 2004). The best-studied example is the brome mosaic virus (BMV) 1a replicase, which localizes to the ER and induces membrane invaginations to form spherules (Lee and Ahlquist, 2003). These invaginations, or spherules, are centers for virus replication and contain the BMV 2a protein and viral RNA (Schwartz et al., 2004). It was suggested that the BMV-induced spherules resemble budding retrovirus cores and that these membrane invaginations containing VRCs have a place in virus evolution (Schwartz et al., 2002, 2004).

Recent information supports the involvement of the endomembrane system in virus intracellular and intercellular movement (for review, see Reichel and Beachy, 1998, 2000; Morozov and Solovyev, 2003; Nelson, 2005; Verchot-Lubicz, 2005). For example, the tobacco mosaic virus (TMV) membrane-bound replication complexes were reported to traffic along the microfilament network with the cell (Liu et al., 2005)

[1] This work was supported by the Noble Foundation, the National Science Foundation (NSF) Integrative Plant Biology Program Award (IBM–9982552), the NSF Multi-user Instrumentation award (DBI–0400580), and the Oklahoma Agriculture Experiment Station (project H–2371).

[2] Present address: Department of Plant and Soil Science, Delaware Biotechnology Institute, Newark, DE 19711.

[3] Present address: Division of Emerging and Transfusion Transmitted Diseases, Center for Biologics Evaluation and Research, Food and Drug Administration, Bethesda, MD 20892.

* Corresponding author; e-mail verchot@okstate.edu; fax 405–744–6039.

Article, publication date, and citation information can be found at www.plantphysiol.org/cgi/doi/10.1104/pp.105.066019.

and then move from cell to cell through the plasmodesmata (Kawakami et al., 2004). The 126- and 183-kD proteins of TMV aid in forming, and are present in, the ER-derived VRCs (Heinlein et al., 1998; Szecsi et al., 1999; Kawakami et al., 2004; Liu et al., 2005). The TMV movement protein associates with the VRCs and at some point is required to transport them across plasmodesmata (Heinlein et al., 1998; Mas and Beachy, 1999; Szecsi et al., 1999; Liu et al., 2005).

Potato virus X (PVX) encodes three movement proteins from a genetic module of three overlapping open reading frames (ORFs), termed the triple gene block. These triple gene block proteins, named TGBp1, TGBp2, and TGBp3, have molecular masses of roughly 25, 12, and 8 kD (Huisman et al., 1988). The PVX TGBp1 protein is a suppressor of gene silencing, an RNA helicase, and gates plasmodesmata (Rouleau et al., 1994; Brigneti et al., 1998; Howard et al., 2004). The TGBp2 and TGBp3 proteins associate with the ER. The results of mutational analyses showed that the association of TGBp2 and TGBp3 proteins with the ER is important for virus infection (Krishnamurthy et al., 2003; Mitra et al., 2003). The PVX coat protein also plays a role in virus movement (Spillane et al., 1997).

In this study, the green fluorescent protein (GFP) gene was fused to the PVX TGBp2 gene to study protein subcellular targeting during virus infection. Time-course experiments were conducted in BY-2 protoplasts and in tobacco leaves to examine the association of the GFP:TGBp2 protein with the ER network during the course of virus infection. We present evidence that the PVX TGBp2 protein, similar to many viral membrane-associated proteins, induces formation of vesicles from the ER. In addition, the PVX TGBp3 protein also associates with the ER. Last, we present evidence that TGBp2-induced vesicles associate with the actin network and are unrelated to the Golgi apparatus.

RESULTS

GFP:TGBp2 Associates with Cellular Membranes during Virus Infection in Protoplasts

The PVX-GFP infectious clone (Fig. 1) expresses the GFP gene from a duplicated coat protein subgenomic promoter. GFP is used as a visual marker to follow virus infection over time. The GFP:TGBp2 fused genes were inserted into the PVX genome in place of the GFP gene to study TGBp2 protein subcellular targeting during virus infection (Fig. 1). Most of the endogenous TGBp2 gene was deleted from the PVX-GFP:TGBp2 infectious clone (Verchot et al., 1998; Fig. 1), and the GFP:TGBp2 fusion provides a functional replacement for the deleted gene.

Infectious PVX-GFP and PVX-GFP:TGBp2 transcripts were inoculated to BY-2 protoplasts, and the subcellular distribution of fluorescence was studied at 18, 24, 36, 48, and 72 h postinoculation (hpi) using confocal microscopy. In PVX-GFP-inoculated protoplasts, fluorescence was mainly cytosolic and nuclear, with no obvious change in the pattern of GFP expression over time (Fig. 2, F and K). These data support related studies in which the GFP protein is typically cytosolic and nuclear when expressed in tobacco

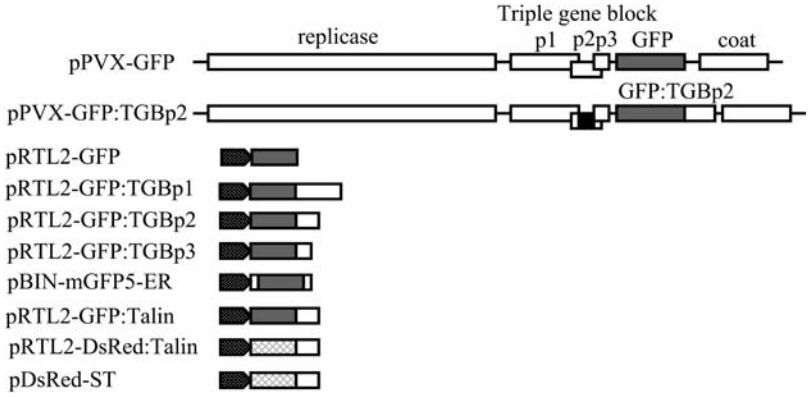

Figure 1. Schematic representation of plasmids used in this study. The pPVX-GFP and pPVX-GFP:TGBp2 plasmids contain the entire PVX genome. The white boxes in these schematics represent the PVX ORFs or subcellular targeting signals, and the lines represent noncoding regions. The names for each PVX gene are indicated above the boxes. The GFP gene (gray box) or GFP:TGBp2-fused genes were inserted into the PVX genome. In the pPVX-GFP:TGBp2 plasmid, a large portion of the endogenous TGBp2 coding sequence was deleted from the PVX genome (indicated by a black box). Four pRTL2 plasmids expressed GFP alone (gray box) or fused to the 5′-end of the PVX TGBp1, TGBp2, or TGBp3 genes (white boxes). The pBIN-mGFP5-ER has sequences encoding ER-targeting and retention signals fused to the 5′- and 3′-ends of the GFP gene. The pRTL2-GFP:Talin and -DsRed:Talin plasmids have the coding sequence of the F-actin-binding domain of mouse Talin (McCann and Craig, 1997; Kost et al., 1998) for actin targeting of GFP or DsRed (hatched box). The pDsRed-ST plasmid has sequences encoding the Golgi-targeting signal of rat ST fused to DsRed (Dixit and Cyr, 2002). The DsRed-ST fusion is in the pCambia1300 vector (Dixit and Cyr, 2002). All pRTL2, pBIN, and pCambia1300 plasmids contain a CaMV 35S promoter (black spotted arrows).

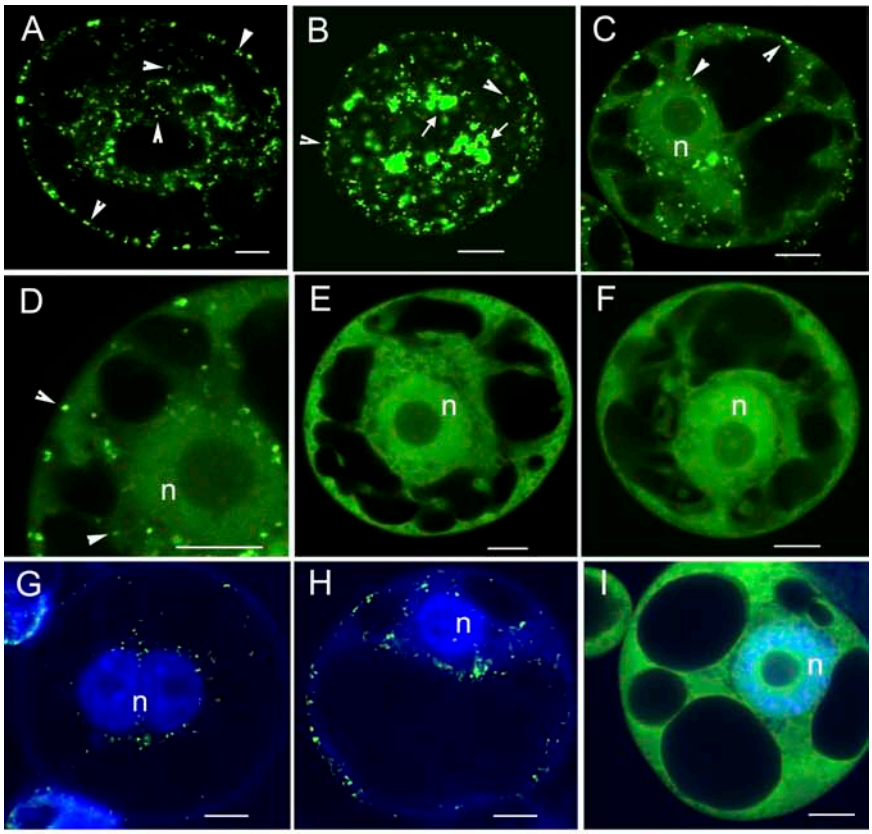

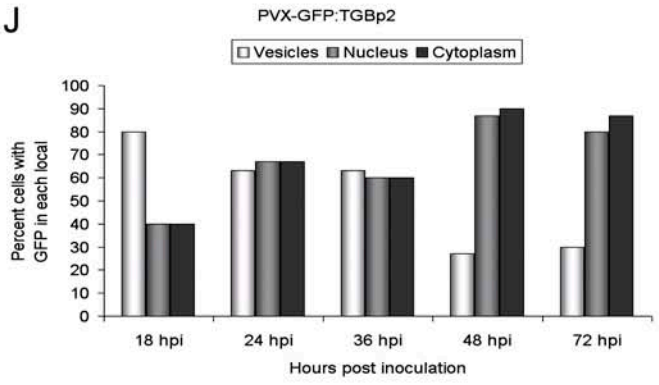

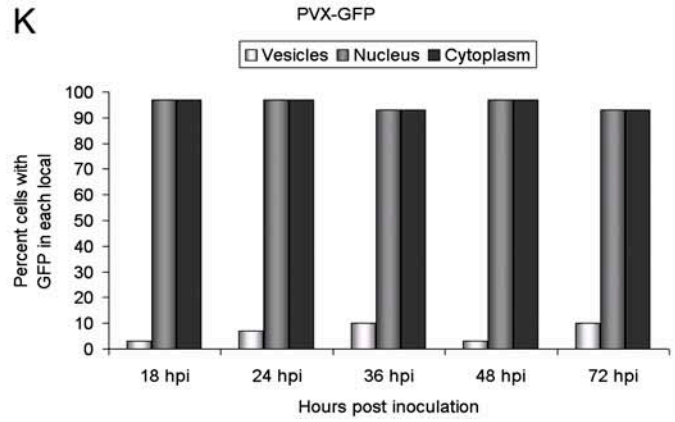

Figure 2. Confocal images of protoplasts infected with PVX-GFP:TGBp2 and PVX-GFP. A to C, PVX-GFP:TGBp2-infected protoplasts show fluorescence in vesicles (A); vesicles and aggregates of vesicles (B); and vesicles, nucleus (n), and cytoplasm (C). D, A magnified portion of the protoplast presented in C. Vesicles appear along the plasma membrane and surrounding the nucleus. E and F, PVX-GFP:TGBp2 (E) and PVX-GFP-infected protoplast (F) show nuclear and cytoplasmic fluorescence. G to I, DAPI-stained protoplasts infected with PVX-GFP:TGBp2. G, Dividing protoplasts have two adjacent nuclei stained with DAPI. GFP fluorescent vesicles surround the nuclei in G and H. I, DAPI-stained cell shows GFP:TGBp2 in the nucleus and cytoplasm. Bars in each photograph represent 10 μm. J, Thirty protoplasts were scored for the presence of fluorescence in vesicles, nucleus, and cytoplasm in PVX-GFP:TGBp2-infected protoplasts at 18, 24, 36, 48, and 72 hpi. K, Thirty protoplasts were scored for the presence of fluorescence in vesicles, nucleus, and cytoplasm in PVX-GFP-infected protoplasts at 18, 24, 36, 48, and 72 hpi. Bars represent the percentage of protoplasts having fluorescence in each subcellular compartment at each time point. Between 1% and 10% of protoplasts at each time point contained GFP in vesicles resembling those seen in the PVX-GFP:TGBp2-infected cells. Logistic regressions were conducted using data in J and K and reported in ''Results.''

leaves and protoplasts (Oparka et al., 1999; Crawford and Zambryski, 2000, 2001; Yang et al., 2000).

There were three patterns of GFP:TGBp2 protein fluorescence noted at each time point: (1) in vesicles only, (2) in vesicles and cytosol, and (3) in cytosol and nucleus (Fig. 2, A–D). The vesicles containing GFP:TGBp2 proteins were perinuclear as well as lining the plasma membrane (Fig. 2, A, C, and D). Vesicles sometimes aggregated (Fig. 2B). GFP:TGBp2 fluorescence associated with the nucleus, but not with the nucleolus, as visualized after 4′,6-diamino-phenylindole (DAPI) staining of protoplasts (Fig. 2, E, G, H, and I).

We quantified the patterns of GFP:TGBp2 protein fluorescence to determine whether the subcellular distribution of GFP:TGBp2 fluorescence changes over time. Thirty protoplasts were scored at each time point for fluorescence associated with the vesicles, nucleus, and/or cytosol (Fig. 2J). The proportion of protoplasts containing GFP:TGBp2 fluorescence in vesicles was 80% at 18 hpi and declined to 27% by 48 hpi. This level was maintained through 72 hpi (Fig. 2J). The proportions of protoplasts containing GFP:TGBp2 fluorescence in the cytosol and nucleus were 40% at 18 hpi and increased to 80% and 90% at 48 and 72 hpi, respectively (Fig. 2J). Thus, GFP:TGBp2 fluorescence associates mainly with vesicles early in virus infection, but increasingly with the cytosol and nucleus as infection progresses (Fig. 2J).

Statistical analyses were performed using the data represented in Figure 2, J and K, to determine whether the subcellular distribution of fluorescence in PVX-GFP:TGBp2- and PVX-GFP-infected protoplasts is regulated over time. Time is a likely variable in studying protein subcellular trafficking. If the TGBp2 proteins traffic from one location to another in the cell, then changes in the distribution of GFP:TGBp2 fluorescence within the cell over time would not be random. For example, movement of the GFP:TGBp2 proteins from vesicles into the cytosol may be regulated by the host degradation machinery. Since GFP:TGBp2 is an ER-associated protein, it is possible that ER stress stimulates export of the GFP:TGBp2 proteins to the cytosol for degradation by the 26S proteasome. It is also possible that movement of the GFP:TGBp2 proteins would be regulated and not random if it is controlled by interactions with other PVX proteins.

Therefore, a logistic regression was used to test whether time is a variable in the subcellular accumulation patterns of GFP:TGBp2 and GFP fluorescence. The presence/absence of fluorescence in each subcellular address (vesicle, nucleus, and cytoplasm; dependent variable) were compared over time (independent variable). We hypothesized that the observed changes in the distribution of GFP:TGBp2 proteins over time would indicate subcellular trafficking of the fusion protein. If time is not a variable controlling the distribution of fluorescence within the cell, then statistical analyses would indicate that the distribution of protein in each subcellular address is independent of time (i.e. random) and no correlation would exist. Slope estimates and P values were determined. A nonsignificant slope (i.e. large P value) indicates no relationship to time. Conversely, a significant slope (i.e. small P value) indicates the response is affected by time. A negative slope indicates a decreased presence of fluorescence in each address over time, and a positive slope indicates an increase of fluorescence in each address over time. For PVX-GFP:TGBp2, the slope values for vesicles, nucleus, and cytoplasm were -0.0367, 0.0313, and 0.0463, respectively. The P values were 0.0001, 0.0014, and 0.0001, respectively. The negative slope for PVX-GFP:TGBp2 in vesicles indicates that fluorescence decreased in these locations over time. The positive slope for PVX-GFP:TGBp2 in the cytoplasm and nucleus indicates fluorescence increased in these locations over time. The extremely low P values indicate that changes in subcellular targeting of GFP:TGBp2 proteins over time were significant. For PVX-GFP, the slope values for vesicles, nucleus, and cytoplasm were 0.0145, -0.0155, and -0.0155, respectively. The P values were 0.3631, 0.4009, and 0.4009, respectively. The nonsignificant slopes and high P values for PVX-GFP indicate that the change in fluorescence at each subcellular address had no relationship to time and was random. Thus, statistical analysis supports the hypothesis that GFP:TGBp2 proteins first resided in vesicles and over time became increasingly cytosolic and nuclear.

Subcellular Targeting of GFP:TGBp2 during Virus Infection of Tobacco Leaves

PVX-GFP and PVX-GFP:TGBp2 transcripts were inoculated to tobacco leaves and fluorescence was examined between 2 and 5 d postinoculation (dpi) to determine whether the pattern of fluorescence observed in tobacco leaves resembles the pattern reported in protoplasts. Within a single infection focus, cells were viewed early and late during virus infection. The intracellular fluorescence patterns located at the leading edge and at the center of infection foci were compared to determine whether the subcellular distribution of fluorescence changed as infections developed. Since tobacco leaf cells are not synchronously infected, we could not use statistical methods to assess changes in the distribution of GFP or GFP:TGBp2 proteins over time.

In PVX-GFP-inoculated leaves, the patterns of fluorescence at the leading edge and at the center of the infection foci were similar. Fluorescence was observed in the cytosol, nucleus, and perinuclear inclusion bodies (Fig. 3, A and B). Sometimes it was difficult to discern between GFP fluorescence inside the nucleus and perinuclear inclusion bodies. These inclusion bodies are likely X-bodies described in early literature as masses containing virus particles, ER, and ribosomes (Kikumoto and Matsui, 1961; Kozar and Sheludko, 1969; Allison and Shalla, 1973). Based on previous reports describing formation of X-bodies (Kikumoto and Matsui, 1961; Kozar and Sheludko,

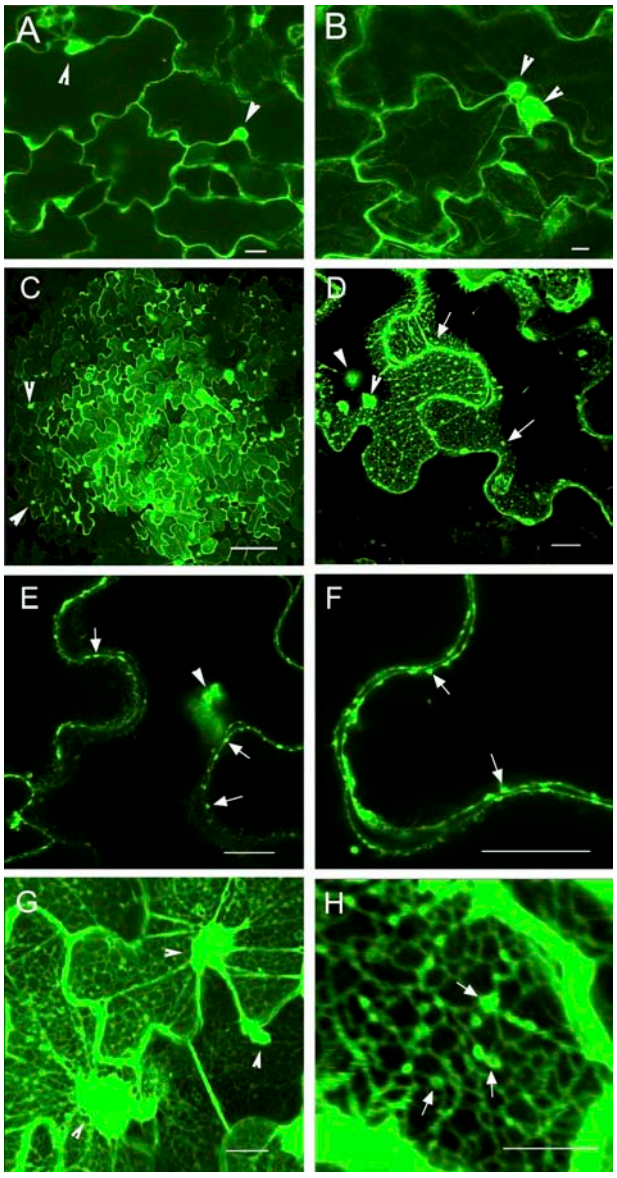

Figure 3. Confocal images of PVX-GFP and PVX-GFP:TGBp2-infected *N. benthamiana* leaf epidermal cells. A and B, PVX-GFP-infected cells at 2 and 6 dpi, respectively. Green fluorescence is present in the cytoplasm and nucleus. There were also perinuclear inclusion bodies that, on occasion, seemed to surround the nucleus. Since the perinuclear inclusions often overlap the nucleus, single arrowheads point to both structures in all images. C to G, PVX-GFP:TGBp2-infected cells at 2 or 4 dpi. Single arrowheads point to inclusion bodies and arrows point to vesicles. C, Image of a PVX-GFP:TGBp2 infection focus taken at low magnification at 4 dpi. D, Image of cells located at the front of an infection focus. Fluorescence was evident in the ER network, vesicles, and inclusion bodies. E and F, Single optical cross-sections through the middle of the cell located at the front of an infection focus. The vesicles appear as twin structures along the walls of opposing cells. G and H, Images of cells located in the center of an infection focus at 4 dpi. These images show fluorescence in a thick layer of cytoplasm around the cell, the ER, and vesicles. The nuclear fluorescence is either due to GFP:TGBp2 accumulating inside the nucleus, perinuclear X-bodies that overwhelm the nucleus (Kikumoto and Matsui, 1961; Kozar and Sheludko, 1969; Allison and Shalla, 1973), or both. Bars in all images, except C, represent 20 μm; bar in C represents 200 μm.

1969; Allison and Shalla, 1973; Espinoza et al., 1991), we postulate the strands extending from these X-bodies to the plasma membrane (Fig. 3, A and B) to be ER derived.

PVX-GFP:TGBp2 infection foci were observed from 2 to 5 dpi. Fluorescence was associated with the ER network and vesicles in all infected cells. Perinuclear inclusion bodies were observed in all infected cells (Fig. 3, C–E). Vesicles appeared to move along the ER strands in tobacco epidermal cells (data not shown). A thick band of cytosolic fluorescence was evident in cells located at the center of infection, but was less obvious at the leading edge of infection. Although the intensity of fluorescence was weaker at the leading edge of infection, the patterns of fluorescence in the ER network and vesicles at this location were similar to those observed in cells at the center of the infection foci (Fig. 3, C–F). Single optical cross-sections taken through the middle of infected cells revealed vesicles lining the cell wall (Fig. 3, E and F). These vesicles were sometimes twin structures along the walls of adjacent cells and resemble the peripheral bodies reported to occur in beet necrotic yellow vein virus (BNYVV; a benyvirus), potato mop top (PMTV; a pomovirus) or the poa semilatent virus (PSLV; a hordeivirus; Erhardt et al., 2000; Solovyev et al., 2000; Gorshkova et al., 2003; Zamyatnin et al., 2004; Haupt et al., 2005) infected cells.

Data obtained in inoculated plants confirmed observations in protoplasts. In early infected cells and protoplasts, the GFP:TGBp2 proteins accumulated mainly in vesicles. In cells and protoplasts infected for a long period of time, we observed an increase in cytosolic fluorescence. In plants, GFP:TGBp2 proteins were found simultaneously in the ER as well as in vesicles. We never obtained evidence that the GFP:TGBp2 proteins move from the ER into vesicles, or from vesicles into the ER. Rather, the data indicate that GFP:TGBp2 proteins are either simultaneously targeted to the ER and cellular vesicles or that the GFP:TGBp2 proteins induce reorganization of the ER soon after translation.

Fluorescence Declines in PVX-Infected Protoplasts following Cycloheximide Treatment

In PVX-GFP:TGBp2-infected plants, we observed GFP:TGBp2 fluorescence in the ER as well as in vesicles, suggesting that the vesicles may be invaginations of the ER network. In protoplasts inoculated with PVX-GFP:TGBp2, fluorescence was redistributed from the vesicles into the cytosol. It is therefore reasonable to consider that ER retention of viral proteins and/or ER reorganization by the TGBp2 protein triggers ER-associated protein degradation as a result of ER stress (Brandizzi et al., 2003; Martinez and Chrispeels, 2003; Smalle and Vierstra, 2004; Kirst et al., 2005). It is also possible that the TGBp2 protein itself is unstable, causing the fusion protein to be targeted to the cytosol for degradation.

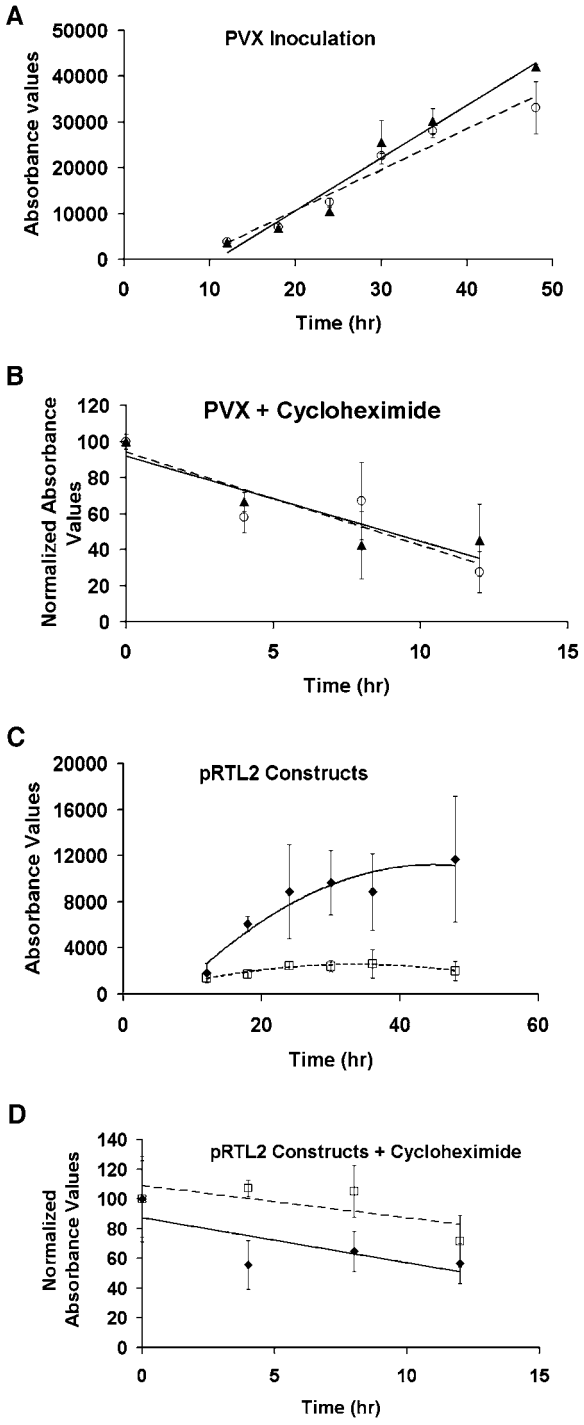

Figure 4. Fluorometric assays measuring GFP fluorescence in BY-2 protoplasts. The averages of three fluorometric values were plotted at each time point. A, PVX-GFP (black triangle) and PVX-GFP:TGBp2 (white circle) infected protoplasts. The average fluorometric values were plotted using linear regression. B, PVX-GFP (black triangles) and PVX-GFP:TGBp2 (white circles) infected protoplasts treated with cycloheximide at 24 hpt. The average fluorometric values were normalized to an average time 0 measurement and then plotted using linear regression. C, pRTL2-GFP (black diamonds) and pRTL2-GFP:TGBp2 (white squares) transfected protoplasts. The average fluorometric values were plotted and a best-fit curve was determined using polynomial regression. D, pRTL2-GFP (black diamonds) and pRTL2-GFP:TGBp2 (white squares) transfected protoplasts were treated with cycloheximide at 24 hpt. The average fluorometric values were normalized to an average time 0 measurement and then plotted using linear regression.

Fluorometric assays were used to quantify GFP expression over time as a measure of both protein accumulation and degradation in BY-2 protoplasts. We then compared the rates of protein turnover in protoplasts inoculated with the PVX viruses with the rates of protein turnover in protoplasts transfected with the pRTL2 plasmids. Inoculated and transfected protoplasts were chased at 24 h with cycloheximide to halt protein synthesis. Fluorometric values were obtained at 0, 4, 8, and 12 h following treatment with cycloheximide and the protein half-lives were calculated. The fluorometric values were normalized to a time 0 measurement. The data were plotted and a linear regression was used to calculate protein half-lives. We predicted that if protein turnover was stimulated as the result of virus infection, then fluorescence would decline more rapidly in virus-infected protoplasts than in pRTL2-transfected protoplasts. On the other hand, if TGBp2 contained a degradation signal, then we would expect greater turnover of GFP:TGBp2 than GFP proteins in both PVX-inoculated and pRTL2-transfected protoplasts.

In protoplasts transfected with PVX-GFP or PVX-GFP:TGBp2 transcripts, there was a linear increase in fluorescence between 12 and 48 hpi (Fig. 4A). The fluorescence values obtained at 48 hpi were between 8- and 12-fold higher than the values obtained at 12 hpi. The plotted fluorometric values for PVX-GFP:TGBp2- and PVX-GFP-infected protoplasts were almost identical to each other during most of the time course (Fig. 4A). Since the decrease in GFP and GFP:TGBp2 fluorescence had similar rates, the stability of GFP is not altered by fusion to the TGBp2 protein (Fig. 4B). The half-lives of GFP and GFP:TGBp2 proteins were similar, 8.9 and 8.6 h, respectively.

In protoplasts transfected with pRTL2-GFP or -GFP:TGBp2 plasmids, fluorescence did not show the same linear increase between 12 and 48 h post-transfection (hpt) as reported for the PVX-GFP- and PVX-GFP:TGBp2-infected protoplasts (compare Fig. 4, A and C). Instead, the fluorometric values obtained for these pRTL2 constructs reached a plateau at approximately 24 hpt (Fig. 4C). The values representing GFP expression were 4-fold greater than the values representing GFP:TGBp2 fluorescence between 24 and 48 hpt (Fig. 4C). This was surprising since the fluorometric values obtained in PVX-GFP- and PVX-GFP:TGBp2-infected protoplasts were not significantly different. Perhaps protein accumulation in these transient assays is different when GFP:TGBp2 is expressed from a DNA or RNA promoter (cauliflower mosaic virus [CaMV] 35S promoter or PVX coat protein subgenomic promoter). Since protein expression reaches a plateau at 24 hpt in protoplasts transfected with pRTL2 constructs but

continues to increase in a linear fashion in PVX-inoculated protoplasts, it is possible that nuclear gene expression from a CaMV 35S promoter is more tightly regulated than cytosolic expression of the same gene(s) from a PVX viral promoter. The rate of decrease in GFP fluorescence following cycloheximide treatment was greater than the rate of decrease in GFP:TGBp2 fluorescence. The half-lives calculated for the GFP and GFP:TGBp2 proteins were 12.4 and 27.1 h, respectively. The GFP:TGBp2 fusion protein was more stable than the nonfused GFP protein (Fig. 4D).

Evidence that the GFP and GFP:TGBp2 proteins have shorter half-lives when expressed from the PVX genome than from pRTL2 constructs indicates that protein degradation is stimulated during virus infection. The half-life of the GFP:TGBp2 protein is 8.6 h when expressed from the PVX genome, and this may account for increasing cytosolic fluorescence during the course of infection, representing the last cellular location during degradation. Since the GFP:TGBp2 protein has a 2- to 3-fold longer half-life when expressed from the pRTL2 plasmid, cytosolic accumulation of fluorescence would be minimal in studies involving these plasmids.

Subcellular Targeting of GFP:TGBp2 and GFP:TGBp3 in Transient Expression Assays

To determine whether the PVX TGBp2 protein itself associates with vesicles in the absence of virus infection, pRTL2-GFP:TGBp2 plasmids were transfected into protoplasts or bombarded to tobacco leaves. For comparison, plasmids expressing GFP, GFP:TGBp3, or mGFP5-ER, which encodes a version of GFP that has an N-terminal basic chitinase signal peptide and a C-terminal HDEL sequence for ER targeting and retention (Siemering et al., 1996), were also used (Fig. 1). The plasmids expressing GFP:TGBp3 or mGFP5-ER were selected because these fusion proteins also associate with the ER and provide a comparison for studying the pattern of GFP:TGBp2 fluorescence. The patterns of green fluorescence in protoplasts and leaves were recorded using confocal microscopy.

Ninety-three percent (28/30) of the protoplasts expressed GFP:TGBp2 in vesicles only, and 13% (4/30) of the protoplasts showed fluorescence in the ER as well as in vesicles associated with the ER (Table I). All cells contained some aggregates of vesicles (Table I; Fig. 5, A–C). As in the PVX-GFP:TGBp2-infected protoplasts, the vesicles or aggregates were either perinuclear or along the plasma membrane (compare Fig. 2, A and B, with Fig. 5A).

Both GFP:TGBp3 and mGFP5-ER proteins were observed in the ER network in protoplasts and tobacco leaves (Fig. 5, E–H). The tubules and branches of the cortical ER network were shorter in protoplasts (Fig. 5, D–H) than in leaf epidermal cells, making the network in BY-2 protoplasts more difficult to resolve microscopically than in intact leaves. The small volume of the protoplasts cause the ER network to appear more compact than it appears in tobacco leaf epidermal cells. We did not observe fluorescent vesicles in protoplasts or tobacco leaf epidermal cells expressing either the GFP:TGBp3 or mGFP5-ER constructs (Table I; data not shown). In protoplasts or bombarded leaves expressing only GFP, fluorescence was cytosolic and nuclear (Table I; Fig. 5, I–J). In comparing the data obtained using GFP:TGBp2, GFP:TGBp3, and mGFP5-ER constructs, it appears that the GFP:TGBp2 proteins have the unique ability to associate with vesicles.

Table I. *Subcellular accumulation of fluorescence in transiently transfected protoplasts*[a]

Construct	Total Cells	Nucleus	Cytosol	ER	Vesicles	Aggregates
GFP	30	30a	30a	0b	NO	NO
mGFP5-ER	15	0b	0b	15a	NO	1b
GFP:TGBp2	30	0b[b]	0b[b]	4b[b]	28a	30a
GFP:TGBp3	30	0c	0c	24b	NO	30a

[a]BY-2 protoplasts were transfected with four GFP constructs, and fluorescence was analyzed 18 hpt using confocal microscopy. Accumulation of fluorescence in the nucleus, cytosol, ER, vesicles, or aggregates was quantified. Aggregates were defined as those occasions when fluorescence appeared in bright amorphous bodies whose structures were sometimes difficult to describe. The pattern of fluorescence was scored for a random set of 15 or 30 cells. Proportions of cells containing fluorescence in the nucleus, cytoplasm, ER, vesicles, and aggregates are compared pairwise with Fisher's exact test. Numbers within a row with the same letter are not significantly different at a 0.05 significance level. [b]Comparison of the 0 values for nucleus and cytosol with the value of 4 for ER had a *P* value of 0.0562 and thus is considered biologically significant.

GFP:TGBp2 Is in ER-Derived Vesicles and GFP:TGBp3 Is in the ER Network

It is common that viral proteins associating with the endomembrane system cause changes in membrane architecture. The PVX TGBp2 protein may cause invaginations of the ER network similar to those caused by the membrane-binding proteins encoded by TMV, BMV, tobacco etch virus, and peanut clump virus (PCV; Schaad et al., 1997; Reichel and Beachy, 1998; Dunoyer et al., 2002; Schwartz et al., 2002, 2004; Lee and Ahlquist, 2003). However, we had not eliminated the possibility that the PVX TGBp2 protein associates with Golgi vesicles.

To determine the origin of the GFP:TGBp2-associated vesicles, we conducted immunogold labeling and electron microscopic analysis of freeze-substituted leaf tissue taken from transgenic tobacco expressing mGFP5-ER, GFP:TGBp2, or GFP:TGBp3 proteins (Figs. 6 and 7; Table II). The mGFP5-ER or GFP:TGBp3 transgenic tobacco was used for comparison because these fusion proteins are known to associate with the ER (Krishnamurthy et al., 2003; Mitra et al., 2003). Immunogold labeling detected GFP in the ER in all three samples. Nontransgenic samples were included in the study as negative controls and showed minimal reaction with the antisera used in this study (Fig. 6; Table II).

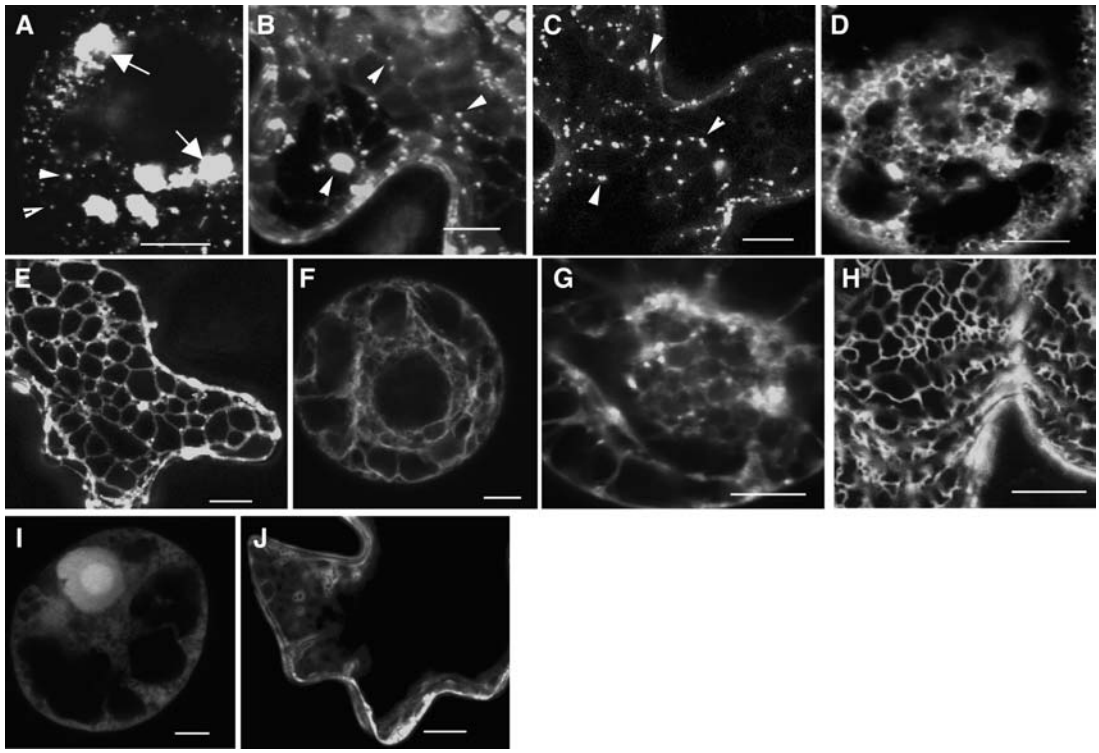

Figure 5. Confocal images showing subcellular accumulation of fluorescent proteins expressed transiently in BY-2 protoplasts and *N. benthamiana* leaves. Arrows point to aggregates and arrowheads point to vesicles in A to C. A, D, F, G, and I, Images of protoplasts. B, C, E, H, and J, Images of tobacco leaf epidermal cells. A to C, pRTL2-GFP:TGBp2-transfected protoplasts and cells. D and E, pRTL2-GFP:TGBp3-transfected protoplasts and cells. F to H, pBIN-mGFP5-ER-transfected protoplasts and cells. D through H show ER network. I and J, pRTL2-GFP-transfected protoplasts and cells. GFP is cytosolic. Bars represent 10 μm.

Immunolabeling was carried out using antiserum against GFP (since antibodies to the PVX TGBp2 and TGBp3 proteins were unavailable) and/or binding protein (BiP; Table II). BiP antisera were chosen because the BiP protein is an ER resident chaperone that is not in other areas of the endomembrane system (Fontes et al., 1991). Ten-nanometer gold particles were associated with GFP antisera, and 25-nm gold particles were associated with BiP antisera in all experiments. The presence of immunogold labeling in the ER, cell wall, and plasma membrane was quantified and compared statistically (Table II). The average numbers of gold particles (of each type) associated with the cell wall, plasma membrane, ER, vesicles, and Golgi apparatus were calculated in 1-μm^2 fields. Gold particles embedded in the cell wall were scored as cell wall particles. Gold particles deposited on the cytosolic side of the cell wall near the plasma membrane were considered to be associated with the plasma membrane.

Immunogold labeling with the GFP and BiP antisera was specific (Table II). In mGFP5-ER or GFP:TGBp3 transgenic samples treated with GFP and/or BiP antisera, the gold particles were mainly along the ER (Fig. 6, A, C, and D, and Fig. 7, D–F; Table II) and were rarely in the plasma membrane, cell wall, or Golgi network. There was minimal label in nontransgenic samples treated with GFP antisera (data not shown; Table II). Only the BiP antisera labeled the ER in nontransgenic cells (Fig. 6G; Table II). Statistical analyses confirm the mGFP5-ER and GFP:TGBp3 fusion proteins localize mainly to the ER network (Table II). Additional controls included treating samples with buffer, TMV antisera, or secondary antisera. There was little or no labeling of the mGFP5-ER, GFP:TGBp2, and GFP:TGBp3 transgenic or nontransgenic samples following any of these treatments (Fig. 6, B–F; nontransgenic data not shown; Table II).

Membrane vesicles were plentiful in GFP:TGBp2-expressing tissues (Fig. 7, A–C), but were absent from mGFP5-ER transgenic, GFP:TGBp3 transgenic, or nontransgenic leaf samples (Table II; Figs. 6 and 7). At high magnification, we saw granules along the outline of many vesicles that we regarded as ribosomes (Fig. 7, A–C). Vesicles were mainly observed in the cortical region of the cell and were often abutting the cell wall (Fig. 7, B and C). Vesicles ranged from 150 to 500 nm in diameter, and the number of vesicles per 1-μm^2 field ranged from 1 to 3. Roughly 70% of the fields analyzed in GFP:TGBp2 samples contained vesicles (Table II).

In GFP:TGBp2 transgenic samples, immunolabeling with GFP was mainly associated with the ER and TGBp2-induced vesicles (Fig. 7, A–C; Table II). In GFP:TGBp3 transgenic samples, GFP and BiP immunolabeling was mainly along the ER (Fig. 7, D–F; Table

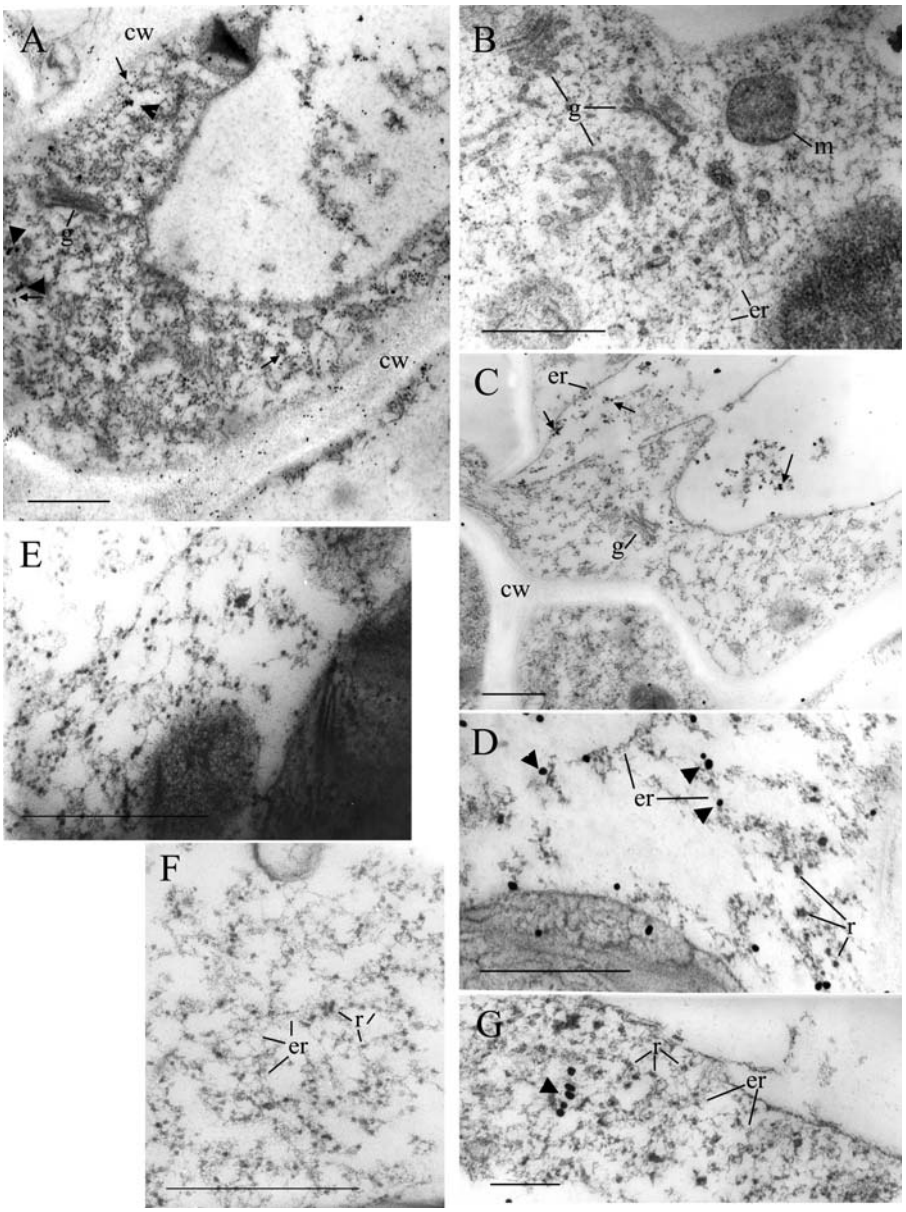

Figure 6. Electron micrographs taken of freeze-substituted transgenic and nontransgenic *N. tabacum* leaf segments following various treatments. Cell wall (cw) mitochondria (m), Golgi stacks (g), ER (er), and ribosomes (r) are indicated. The long black and arrows point to GFP-labeled ultrastructures, and the black and arrowheads point to BiP-labeled ultrastructures. A to D, mGFP5-ER transgenic cells. A and D, mGFP5-ER transgenic tobacco cells probed with both GFP (10 nm gold) and BiP (20 nm gold) antiserum. B, mGFP5-ER transgenic cells treated with buffer and secondary antisera have no label in the ER. C, mGFP5-ER transgenic cells treated with GFP antisera show label associated with the ER. E, GFP:TGBp2 transgenic cell treated with buffer and secondary antisera. F, GFP:TGBp3 transgenic cell treated with buffer and secondary antisera. G, Nontransgenic cell treated with BiP antiserum. Bars represent 0.5 μm.

II). In both GFP:TGBp2 and GFP:TGBp3 samples, gold particles were rarely present in the cell wall, plasma membrane, or Golgi apparatus (Fig. 7, B and C; Table II). These data indicate that GFP:TGBp2 and GFP:TGBp3 are ER-associated proteins when expressed alone. The vesicles seen in GFP:TGBp2 transgenic cells were never present in GFP:TGBp3, mGFP5-ER, or nontransgenic leaves, suggesting that they are TGBp2-induced structures. Immunogold labeling indicated that GFP:TGBp2 proteins associate with these vesicles. Since these vesicles were specific to GFP:TGBp2-expressing samples and were studded with ribosomes (Fig. 7, A and C), it is likely the GFP:TGBp2 protein induced reorganization of the ER to produce these structures.

Bombarded Cells Treated with Brefeldin A or Latrunculin B

Brefeldin A (BFA) causes Golgi proteins to redistribute into the ER and impedes transport vesicles from cycling between the two compartments (Brandizzi et al., 2002; Nebenfuhr et al., 2002). High BFA concentrations cause the formation of Golgi-ER hybrid compartments (Nebenfuhr et al., 2002; Ritzenthaler et al., 2002). If the TGBp2-induced vesicles were Golgi related, we expect that BFA treatment of GFP:TGBp2-expressing tissue would eliminate vesicles and disrupt the ER-Golgi network. If the GFP:TGBp2-induced vesicles were produced by redistribution of the ER membranes, as indicated by the results of electron

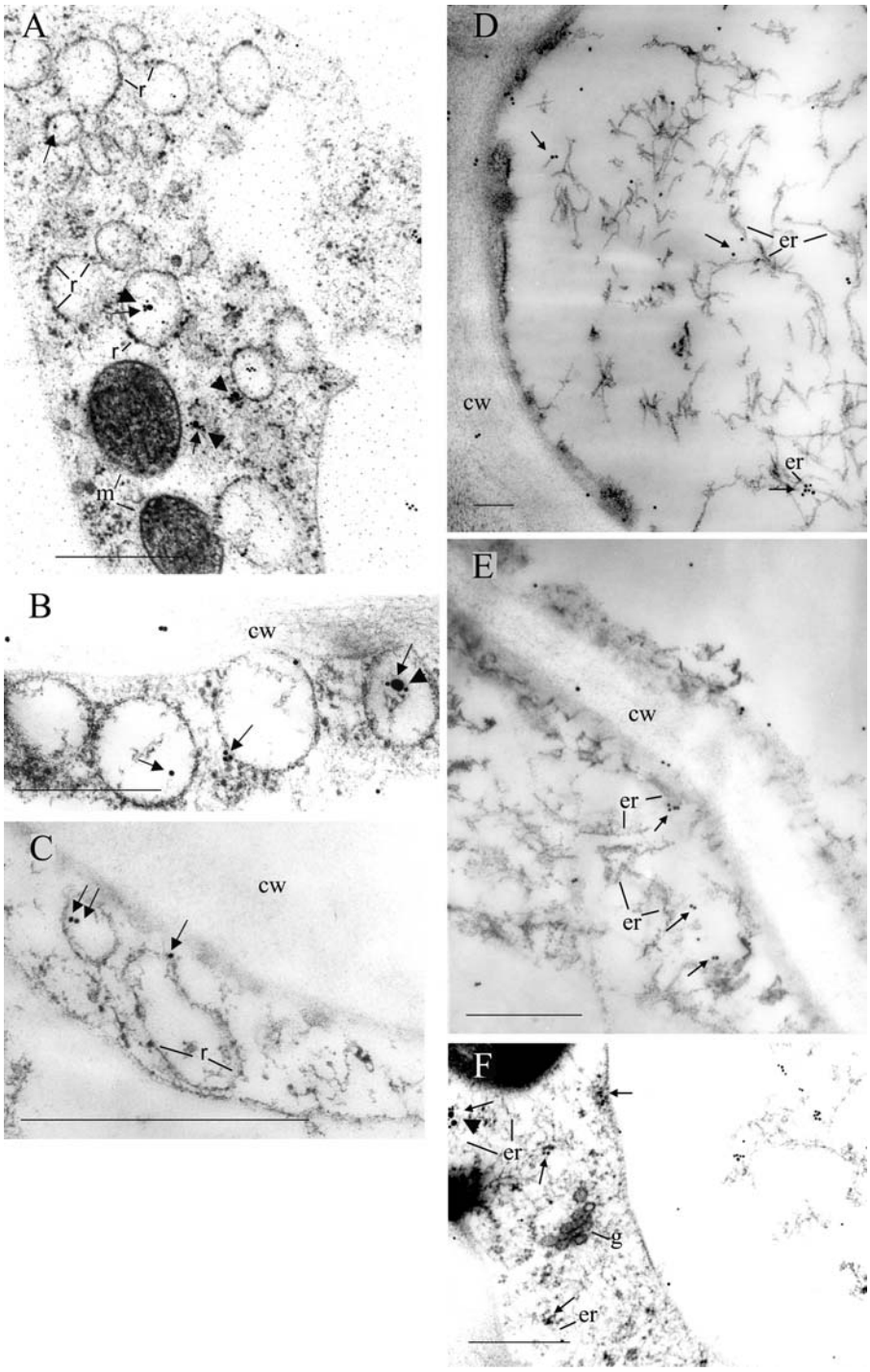

Figure 7. Electron micrographs of freeze-substituted GFP:TGBp2 and GFP:TGBp3 transgenic *N. tabacum* leaf segments with various treatments. The 10-nm gold particles associated with GFP antiserum are indicated by long black arrows. The 20-nm gold particles associated with BiP antiserum are indicated by black arrowheads. The mitochondria (m), chloroplast (chl), cell wall (cw), Golgi apparatus (g), ER (er), and ribosomes (r) are indicated. A to C, GFP:TGBp2 transgenic cells show vesicles. Some vesicles lay along the cell wall. D to F, GFP:TGBp3 transgenic cells. A, C, D, and E, Samples treated with GFP antisera. B and F, Samples treated with GFP and BiP antiserum. Bars represent 0.5 μm.

microscopy, then BFA treatment would not alter the presence of these vesicles within the cell.

GFP:TGBp2-, GFP:TGBp3-, and mGFP5-ER-expressing leaf segments were treated with 200 μg mL^{-1} BFA for 3 to 4 h (Ritzenthaler et al., 2002; Saint-Jore et al., 2002; Krishnamurthy et al., 2003; Mitra et al., 2003). While nontreated leaves expressing GFP:TGBp2 displayed typical granular-type vesicles, as well as the reticulate network (Fig. 8C), in BFA-treated cells the ER network was dissolved into patches of membranes and the small granular-type vesicles remained distributed throughout the cell (Fig. 8F). Since BFA treatment was not disruptive to the vesicles containing GFP:TGBp2 proteins (Fig. 8F), it is not likely that these were Golgi vesicles. In mGFP5-ER- and in GFP:TGBp3-expressing cells treated with BFA, the ER network is dissolved and there are large and small patches of fluorescence scattered throughout the cells (Fig. 8, D

Table II. *Distribution of immunogold labeling with GFP, BiP, and TMV antiserum in transgenic N. tabacum leaves*

Transgene[a]	Antisera[b]	Fields[c]	Total CW	Mean ± SE of Number of Gold Particles in:[d]			
				PM	ER	Golgi[e]	Vesicles[f]
Experiments using single antisera							
GFP:TGBp2	GFP	41	0.8 + 0.3b	0.3 + 0.1b	3.4 ± 0.5a	0 ± 0b	1.3 ± 0.5b
GFP:TGBp3	GFP	31	0.8 ± 0.4b	0.7 ± 0.4b	4.3 ± 0.7a	0 ± 0b	NO
mGFP5-ER	GFP	37	0.4 ± 0.2b	0.1 ± 0.1b	2.4 ± 0.4a	0.4 ± 0.2b	NO
Nontransgenic	GFP	36	0.3 ± 0.1a	0.2 ± 0.1a	0.3 ± 0.1a	0 ± 0a	NO
GFP:TGBp2	BiP	8	0.3 ± 0.3b	1.4 ± 0.5a	1.6 ± 0.5a	–	–
GFP:TGBp3	BiP	12	0 ± 0b	0.3 ± 0.2b	2.5 ± 0.3a	–	NO
mGFP5-ER	BiP	12	0 ± 0b	0.1 ± 0.1b	1.5 ± 0.3a	–	NO
Nontransgenic	BiP	15	0.1 ± 0.1b	0.4 ± 0.2b	2.3 ± 0.4a	–	NO
GFP:TGBp2	NoAb	22	0 ± 0a	0 ± 0a	0 ± 0a	–	–
GFP:TGBp3	NoAb	20	0 ± 0a	0 ± 0a	0.1 ± 0.1a	–	–
mGFP5-ER	NoAb	13	0 ± 0b	0 ± 0b	0.6 ± 0.2a	–	–
Nontransgenic	NoAb	10	0 ± 0a	0 ± 0a	0 ± 0a	–	–
Experiments using two antisera							
GFP:TGBp2	GFP	51	0.8 ± 0.2b	1.1 ± 0.2b	3.5 ± 0.4a	0 ± 0b	2.6 ± 0.2b
	BiP	51	0 ± 0c	0.2 ± 0.1c	0.6 ± 0.1a	0 ± 0c	0.3 ± 0.1b
GFP:TGBp3	GFP	28	1.1 ± 0.6b	0.4 ± 0.2b	7.3 ± 0.9a	0.4 ± 0.4b	NO
	BiP	28	0.2 ± 0.1b	0 ± 0b	1.2 ± 0.2a	0.0 ± 0b	NO
mGFP5-ER	GFP	29	2.0 ± 0.6b	1.3 ± 0.4b	9.1 ± 0.7a	0.3 ± 0.2b	NO
	BiP	29	0 ± 0b	0.1 ± 0.1b	1.5 ± 0.3a	0.0 ± 0.0b	NO
GFP:TGBp2	GFP	16	0.1 ± 0.1b	0 ± 0b	4.6 ± 1.1a	–	–
	TMV	16	0 ± 0a	0 ± 0a	0 ± 0a	–	–
GFP:TGBp3	GFP	17	1.2 ± 0.6b	0.5 ± 0.3b	5.8 ± 1.0a	–	NO
	TMV	17	0 ± 0a	0 ± 0a	0 ± 0a	–	NO
mGFP5-ER	GFP	13	0 ± 0b	0 ± 0b	0.6 ± 0.2a	–	NO
	TMV	13	0 ± 0a	0 ± 0a	0 ± 0a	–	NO

[a]Transgenic tobacco leaf samples were embedded in LR White, sectioned, and analyzed by immunogold labeling and electron microscopy to assess the subcellular accumulation patterns of GFP:TGBp2 and GFP:TGBp3. Control samples included nontransgenic leaves and transgenic leaves expressing GFP targeted to the ER (mGFP5-ER). Since we lack antisera to PVX TGBp2 and TGBp3, transgenic plants expressing GFP-fused genes were used. Immunogold labeling was then conducted using commercially available anti-GFP sera. [b]In the top half of the table, samples of transgenic or nontransgenic tobacco leaves were treated with either full-length mouse monoclonal AV antiserum (BD living colors; CLONTECH Laboratories) to detect GFP, BiP antiserum, or no primary antiserum (NoAb). All samples were treated with 10-nm gold-conjugated anti-mouse or anti-rabbit sera. In the bottom half of the table, samples were dual-labeled using antiserum to detect GFP and BiP. As a control, some samples were treated with antiserum to detect GFP and TMV. These samples were treated with 10 nm and 25 nm of gold-conjugated anti-mouse and anti-rabbit sera. [c]Fields are defined as areas of 1 μm^2 (using an ultrastructure size calculator) that contain gold particles. Gold particles in each field were counted manually. The total numbers of fields analyzed for each transgenic plant sample are indicated. [d]The numbers of gold particles detected in the cell wall (CW), plasma membrane (PM), and ER were determined for all fields treated with each antiserum. Means within the same row with the same letter are not significantly different using Fisher's protected LSD procedure at a 0.05 significance level on square-root-transformed data. Zeros indicate samples that had the CW, PM, or ER, but no labeling. [e]There were few Golgi viewed in all of the samples analyzed. The averages shown in this table were derived from 5 to 6 Golgi for each sample. –, Antibody treatments in which their reaction with Golgi was not quantified. [f]The vesicles reported in GFP:TGBp2 samples were abundant. Of the total fields analyzed (41 treated with one antiserum and 51 treated with two antisera), there were a total of 72 vesicles viewed. –, Treatments in which the reaction of the antibodies with vesicles was not quantified. NO, None observed.

and E). Nontreated leaves expressing mGFP5-ER or GFP:TGBp3 displayed the reticulate pattern typical of the ER network (Fig. 8, A–C).

Previous studies have shown that movement is facilitated by interactions with the actin microfilaments (Heinlein et al., 1995; McLean et al., 1995; Liu et al., 2005). While the immunogold experiments indicate that the GFP:TGBp2-induced vesicles are ER derived, we were uncertain whether these vesicles associate with the actin network. To further characterize the behavior of these GFP:TGBp2-induced vesicles, leaf segments expressing GFP:TGBp2 were treated with latrunculin B, which is a potent disrupter of actin filaments (Nebenfuhr et al., 1999; Ritzenthaler et al., 2002). Latrunculin B also has minor effects on the shape of the ER, causing an increase in cisternal ER and blind-ending tubules (Knebel, et al., 1990; Nebenfuhr et al., 1999; Brandizzi et al., 2003).

Leaf segments expressing GFP:TGBp2, GFP:TGBp3, mGFP5-ER, or GFP:TGBp3 were treated for 1 to 2 h with latrunculin B. The reticulate pattern typical of the ER network was absent from GFP:TGBp2-expressing cells treated with latrunculin B (Fig. 8I). Instead, we saw GFP:TGBp2-containing vesicles in aggregates, which appeared as many pinwheels within a cell (Fig. 8I). The vesicles seemed to coalesce as a result of latrunculin B disruption of the actin network. The

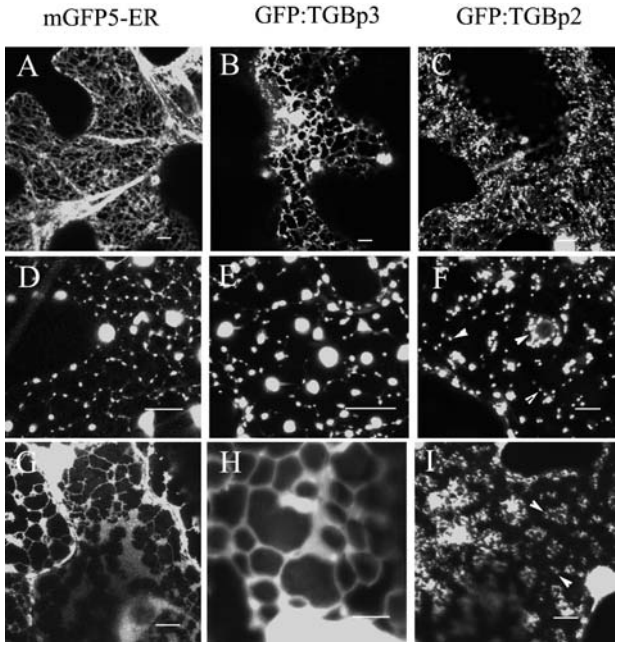

Figure 8. Confocal images are of *N. benthamiana* leaves bombarded with pRTL2-mGFP5-ER, GFP:TGBp2, and GFP:TGBp3 and treated with BFA or latrunculin B. Untreated cells transformed with mGFP5-ER (A); GFP:TGBp3 (B); or GFP:TGBp2 (C). D to F, mGFP5-ER-, GFP:TGBp3-, and GFP:TGBp2-expressing leaves treated with BFA, respectively. G to I, mGFP5-ER-, GFP:TGBp3-, and GFP:TGBp2-expressing leaves treated with latrunculin B, respectively. Arrowheads point to vesicles. Bars represent 10 μm.

pattern of fluorescence in GFP:TGBp2 differed from GFP:TGBp3 and mGFP5-ER cells treated with latrunculin B. In the mGFP5-ER and GFP:TGBp3 samples treated with latrunculin B, the cisternal ER was more prevalent than the tubular ER (Fig. 8, G and H). In both the mGFP5-ER and GFP:TGBp3 samples treated with latrunculin B, the tubules of the ER have fewer branches (Fig. 8, G and H).

Colocalization of GFP:TGBp2 with Actin, Golgi, and GFP:TGBp1

To further examine the association of GFP:TGBp2-induced vesicles and actin filaments, tobacco leaves were bombarded with plasmids expressing GFP:TGBp2 and either DsRed:Talin or GFP:Talin. DsRed:Talin- and GFP:Talin-expressing cells displayed filamentous arrays typical of the actin network (Fig. 9, A–E). Higher magnification images clearly showed GFP:TGBp2-containing vesicles along the length of the red- or green-labeled actin filaments (Fig. 9, B–E). When these cells were treated with latrunculin B, the actin network dissolved and GFP:TGBp2 vesicles were dispersed in the cytosol (Fig. 9F).

Although immunogold labeling indicates that the TGBp2-induced vesicles are primarily associated with the ER, confocal images suggest that the GFP:TGBp2 vesicles resemble the pattern of Golgi vesicles reported in previous studies (Boevink et al., 1998; Saint-Jore et al., 2002). To validate the immunogold-labeling experiments, we cobombarded plasmids expressing GFP:TGBp2 and DsRed-sialyl transferase (ST) to tobacco leaves. DsRed-ST has the signal anchor of a rat ST fused to DsRed-2 and is targeted to the Golgi apparatus (Dixit and Cyr, 2002). The red and green fluorescent vesicles observed in bombarded cells were due to DsRed-ST and GFP:TGBp2 expression, respectively, in cobombarded cells (Fig. 9, G–J). However, the DsRed and GFP signals did not overlap, demonstrating that GFP:TGBp2 did not localize to the Golgi network (Fig. 9, G–J), consistent with the results from our immunogold-labeling studies.

While the cycloheximide chase experiments support the hypothesis that the PVX TGBp2 protein accumulates in the cytosol and nucleus as a result of protein degradation, we could not rule out the possibility that the TGBp2 protein was redirected to the cytosol by other PVX proteins. This hypothesis is also supported by the finding that GFP:TGBp2 is cytosolic when expressed from the PVX genome, but is not cytosolic when expressed from pRTL2 plasmids. For example, in protoplasts expressing only GFP:TGBp2, we saw vesicles and aggregates of vesicles (Fig. 9K). In protoplasts expressing only GFP:TGBp1, fluorescence was nuclear and cytosolic (Fig. 9L). It is possible that, if TGBp1 and TGBp2 interact during virus infection, some populations of GFP:TGBp2 could appear to be nuclear and cytosolic as well. Further investigation is needed to explore the effects of viral protein-protein interactions on their subcellular accumulation patterns.

DISCUSSION

There are several reports that the TGBp2 and TGBp3 proteins of PSLV, BNYVV, and PMTV associate with the ER and with peripheral bodies (sometimes called punctate bodies; Erhardt et al., 2000; Solovyev et al., 2000; Cowan et al., 2002; Gorshkova et al., 2003; Morozov and Solovyev, 2003; Zamyatnin et al., 2004; Haupt et al., 2005). Since studies were conducted using confocal microscopy, the nature of the peripheral bodies was a source of speculation. Some have speculated that these peripheral bodies are vesicles similar to Golgi vesicles (Morozov and Solovyev, 2003). The peripheral bodies observed in studies involving BNYVV, PMTV, and PSLV were sometimes described as twin structures forming on opposite walls of adjacent cells, as seen in this study in PVX-infected cells (Fig. 3, D and E; Erhardt et al., 2000; Solovyev et al., 2000; Cowan et al., 2002; Gorshkova et al., 2003; Morozov and Solovyev, 2003; Zamyatnin et al., 2004; Haupt et al., 2005). This observation has led to the suggestion that these viruses use the secretory pathway to move within the cell toward the plasmodesmata (Morozov and Solovyev, 2003). Here, we

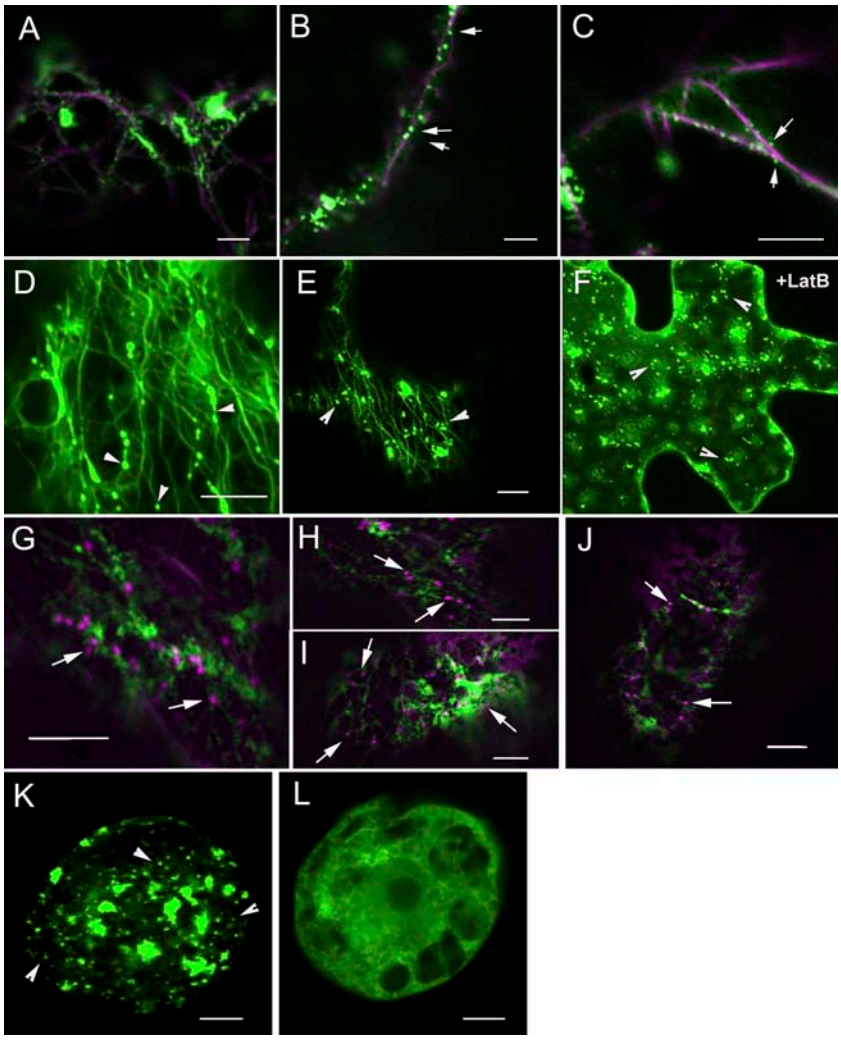

Figure 9. Confocal images showing localization of GFP:TGBp2 with actin, Golgi, and localization of GFP:TGBp1. A to C, Cells expressing GFP:TGBp2 and DsRed:Talin. Arrows point to vesicles along actin filaments. D to F, Cells expressing GFP:TGBp2 and GFP:Talin. Yellow arrowheads point to vesicles. F, Vesicles in cells treated with latrunculin B. G to J, Tobacco epidermal cells cobombarded with GFP-TGBp2 and DsRed-ST. Note that the GFP-TGBp2 vesicles (arrowhead) do not colocalize with the DsRed-ST decorated Golgi (arrows). K, Cells expressing GFP:TGBp2. L, Cells expressing GFP:TGBp1. Bars represent 10 μm.

demonstrated that the PVX TGBp2 protein induces similar peripheral bodies that could be seen under the confocal and electron microscope (Figs. 2, 3, 5, and 7). GFP:TGBp2 was observed in the ER and in vesicles in PVX-GFP:TGBp2-infected protoplasts and tobacco plants, in pRTL2-GFP:TGBp2-transfected protoplasts and bombarded tobacco leaves, and in GFP:TGBp2 transgenic tobacco leaves. Vesicles were not observed in mGFP5-ER- or GFP:TGBp3-expressing samples, suggesting that these vesicles were uniquely induced by the GFP:TGBp2 protein.

Using three different experimental systems, new evidence was obtained indicating that the peripheral bodies induced by the PVX TGBp2 protein are vesicles resulting from invagination of the ER network and are unrelated to the Golgi apparatus. By electron microscopy, it was determined that the vesicles were sometimes studded with ribosomes, suggesting that they were ER derived (Fig. 7, A–C). BiP and GFP antisera colabeled vesicles in GFP:TGBp2 transgenic tissues. Immunolabeling using GFP antiserum did not detect GFP:TGBp2 along the Golgi apparatus, indicating that these vesicles were not likely to be Golgi related (Table II). Further evidence that these vesicles were not related to the Golgi apparatus was obtained in transient expression studies using the Golgi marker DsRed-ST or treatment with BFA (Figs. 8 and 9). These combined data provide further evidence that the vesicles were more likely to be derived from the ER network rather than the Golgi apparatus.

The peripheral bodies reported for PSLV were induced by the TGBp3 protein (Solovyev et al., 2000). Similar bodies were reported for PMTV to be induced by both TGBp2 and TGBp3 (Haupt et al., 2005). In this study, the PVX TGBp2 protein, but not the TGBp3 protein, induces similar structures. Differences among the PSLV, PMTV, and PVX TGBp3 proteins in their abilities to induce vesicles might be the result of evolutionary divergence. In fact, amino acid sequence analyses of many triple gene block-containing viruses suggest that the TGBp2 and TGBp3 proteins of potexviruses and hordeiviruses diverge. The hordeivirus and pomovirus TGBp3 proteins have two transmembrane domains, similar to the potexvirus TGBp2 pro-

tein. The potexvirus TGBp3 has a single transmembrane domain and has a smaller M_r than the hordeivirus and pomovirus TGBp3 proteins (Morozov and Solovyev, 2003; Verchot-Lubicz, 2005). The amino acid sequences show little conservation among the TGBp2 and TGBp3 proteins of hordei-like and potex-like viruses (Morozov and Solovyev, 2003; Verchot-Lubicz, 2005). While these proteins clearly diverge at the amino acid sequence level, it is also possible that divergence of the potex-like viruses and hordei-like viruses may include differences in their interactions with the cellular endomembrane system.

The association of PVX TGBp2 with the actin cytoskeleton and ER, but not with the Golgi, is consistent with recent results with the PMTV TGBp2/3 complex (Haupt et al., 2005). PMTV TGBp2 and TGBp3 showed early localization with the ER network and eventually induced the formation of motile granules that aligned along actin filaments. Moreover, colocalization of the PMTV TGBp2/3 complex with a variety of fluorescent markers late in virus infection implicated the endocytic pathway in recycling some of the viral proteins during virus infection (Haupt et al., 2005). Further research is needed to determine whether intracellular movement of PVX, similar to PMTV, uses the endocytotic pathway for protein recycling.

Viral proteins that are known to associate with cellular membranes often cause changes in the endomembrane architecture (Schwartz et al., 2002; Lee and Ahlquist, 2003). As mentioned in the introduction, VRCs reported for bromoviruses, potyviruses, comoviruses, and dianthoviruses are derived from invagination of the cortical ER (Schaad et al., 1997; Carette et al., 2002a, 2002b; Schwartz et al., 2002; Turner et al., 2004). In the case of TMV, the viral movement protein and the 126- and 183-kD proteins are present in these membrane-bound VRCs, which traffic on microfilaments and move to the plasmodesmata (Kawakami et al., 2004; Liu et al., 2005). The PCV (a pecluvirus) is a triple gene block-containing virus whose replication

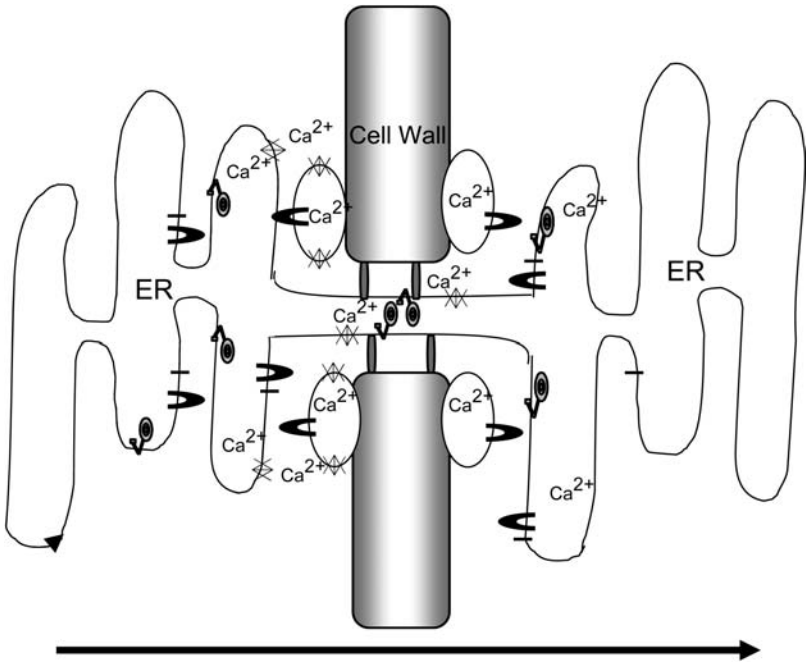

Figure 10. Model linking the ER stress response with virus movement. TGBp2 (black horseshoe) and TGBp3 (black bar) are located in the ER. TGBp2 is also located in ER-derived vesicles located at the periphery of the cell. During PVX infection, TGBp2 is located in vesicles and in the ER in cells located at the infection front and at the center of the infection foci (this study). We do not know whether TGBp3 colocalizes with TGBp2 in the ER-derived vesicles during PVX infection. The ER traverses the plasmodesmata and is a rich store of Ca^{2+} ions. Calmodulin (indicated by gray sphere with a bent arm) is resident in the ER and plasmodesmata and is one example of a factor that controls fluctuations of Ca^{2+} across the ER. The ER-derived vesicles line the cell wall and may also be Ca^{2+} stores. Unconventional myosin VIII (gray bars) is a component of plasmodesmata that regulates gating. Mobilization of calcium, perhaps as a result of ER stress, controls unconventional myosin VIII activities within the plasmodesmata. ER stress may be caused by TGBp2-induced ER reorganization. We do not yet know whether other PVX proteins associate with the TGBp2-induced vesicles, although it is known that TGBp2 and TGBp3 from PMTV colocalize in vesicles (Haupt et al., 2005). If the viral movement complex is associated with the TGBp2-induced vesicles, then it is possible the vesicles move across the plasmodesmata similar to the TMV VRCs. It is also possible that the viral movement complex is exported from the ER (or vesicles) and then moves across the plasmodesmata. Further research is needed to determine the role of the ER, ER stress, and calcium signaling in virus cell-to-cell transport. Arrow at the bottom indicates direction of virus movement from one cell into the adjacent cell.

complex associates with ER-derived vesicles (Dunoyer et al., 2002). These PCV-induced vesicles resemble the vesicles induced by the PVX TGBp2 protein (Dunoyer et al., 2002). While there is no evidence that the PVX TGBp2 protein contributes to virus replication, the TGBp2 protein could potentially colocalize with the viral replicase to mediate transport of membrane-bound PVX VRCs, similar to the TMV VRCs (Kawakami et al., 2004; Liu et al., 2005). Further experiments are needed to determine whether other PVX proteins and PVX RNAs associate with these vesicles.

We observed GFP:TGBp2 in the cytosol and nucleus during PVX infection but not when GFP:TGBp2 was expressed from pRTL2 plasmids. Statistical analysis of the data presented in Figure 2 support the hypothesis that the GFP:TGBp2 protein was redirected to the cytosol by either viral or cellular factors. The pattern of fluorescence observed in protoplasts expressing GFP:TGBp1 was somewhat similar to the pattern of fluorescence observed in PVX-GFP:TGBp2-infected cells (compare Fig. 9L with Fig. 2, C and D). Presently, very little is known regarding interactions among the triple gene block proteins. Further research is needed to learn whether protein subcellular targeting is affected by viral protein-protein interactions.

Another explanation for cytosolic and nuclear accumulation of GFP:TGBp2 relates to the increased levels of protein turnover observed in protoplasts infected with PVX (Brandizzi et al., 2003). Both GFP and GFP:TGBp2 proteins had shorter half-lives when they were expressed from the PVX genome than when they were expressed from pRTL2 plasmids (Fig. 4). Either PVX infection, PVX RNA, or other PVX proteins stimulated protein degradation. Since the TGBp3 protein is also linked to the ER, it is possible that either TGBp3 or a combination of viral proteins can stimulate ER stress responses such as protein export from the ER, protein degradation by the 26S proteasome (ER-associated protein degradation), and fluctuations in ER calcium stores (Navazio et al., 2001; Martinez and Chrispeels, 2003; Smalle and Vierstra, 2004; Kirst et al., 2005).

The TMV movement protein and the turnip yellow mosaic virus movement proteins are degraded by the 26S proteasome (Reichel and Beachy, 2000; Drugeon and Jupin, 2002; Gillespie et al., 2002). In the case of TMV, protein degradation by the 26S proteasome regulates virus movement across the plasmodesmata (Reichel and Beachy, 2000; Gillespie et al., 2002). In fact, a TMV movement protein that was modified by DNA shuffling showed improved transport functions due to its ability to evade proteasome degradation (Gillespie et al., 2002). Protein degradation by the 26S proteasome helps to maintain the integrity of the ER and restore homeostasis in the cell (Reichel and Beachy, 2000). Evidence that GFP:TGBp2 has a longer half-life than GFP in pRTL2-transfected protoplasts suggests that TGBp2 has an ability to evade the proteasome or other protein degradation machinery, thereby moving across the plasmodesmata (Reichel and Beachy, 2000). This may account for cytosolic accumulation of TGBp2 late in infection. Evidence that protein translocation out of the ER is independent of proteasomal degradation was presented in a study of ricin A degradation in which cytosolic protein accumulation was detected following treatment of cells with a proteasome inhibitor (Di Cola et al., 2001). Thus, the ER stress response may play a role in plasmodesmata transport by translocating the PVX TGBp2 or viral movement complexes into the cytosol. The viral movement complex might evade degradation by the 26S proteasome by moving across the plasmodesmata (Reichel and Beachy, 2000; Drugeon and Jupin, 2002; Gillespie et al., 2002).

A model was proposed in which the regulation of calcium stores in the ER by calreticulin controls unconventional myosin VIII activities within the plasmodesmata and thereby controls plasmodesmata gating (Baluska et al., 1999; Reichelt et al., 1999). To expand on this model, it is possible that ER stress responses to virus infection cause calreticulin to release calcium stores, thereby modulating plasmodesmata gating (Fig. 10). Formation of TGBp2-induced vesicles might deplete the ER of calcium stores, causing an influx of calcium into the ER as the cell tries to regain homeostasis. If myosin within the plasmodesmata controls plasmodesmata gating, then fluctuations in calcium levels induced by ER stress and virus infection could also regulate virus cell-to-cell movement. Plasmodesmata gating might allow transport of the TGBp2-induced vesicles across the plasmodesmata. Alternatively, plasmodesmata gating coincides with translocation of PVX proteins out of the ER as a result of ER stress responses. To speculate further, the PVX movement complex might evade 26S proteasome degradation and move across the plasmodesmata (Fig. 10).

To test this model, further research is needed to determine whether PVX infection triggers ER stress responses and whether there is a link between ER stress response and plasmodesmata gating. The ability of virus infection to cause fluctuations in calcium levels across the ER is also worthy of further investigation.

MATERIALS AND METHODS

Bacterial Strains and Plasmids

All plasmids were constructed using *Escherichia coli* strain JM109 (Sambrook et al., 1989). The plasmids pPVX-GFP and pPVX12D-GFP are infectious clones of PVX containing the bacteriophage T7 promoter and the enhanced GFP gene inserted into the PVX cDNA (Fig. 1; Verchot et al., 1998; Krishnamurthy et al., 2003; Mitra et al., 2003). The pPVX12D-GFP plasmid lacks the entire coding sequences for the PVX TGBp2 ORF between nucleotide positions 5,170 to 5,423 and was prepared previously (Verchot et al., 1998). The pPVX-GFP:TGBp2 infectious clone was prepared by replacing the GFP gene in the pPVX12D-GFP infectious clone with the GFP:TGBp2-fused genes. This was accomplished in three steps. First, the GFP:TGBp2 fusion was PCR amplified using the pRTL2-GFP:TGBp2 plasmid. A forward GFP primer (CAG CTA GCA TCG ATG GTG AGC AAG GGC GAG GAG CTG) containing a *Cla*I restriction site (underlined) and reverse primer overlapping the TGBp2 (GGC GGT CGA CAT CTA ATG ACT GCT ATG ATT GTT) sequence and containing a *Sal*I restriction site

(underlined) were used. The PCR products were ligated to pGEMT plasmids (Promega, Madison, WI). In the second cloning step, the GFP:TGBp2 fusion was introduced into pCXS-GFP constructs, which contain a single *Sal*I site (pPVX-GFP constructs contain two *Sal*I sites). The pGEMT-GFP:TGBp2 and pCXS-GFP plasmids were each digested with *Cla*I and *Sal*I restriction enzymes, gel purified, and then ligated. In the third cloning step, the pCXS-GFP:TGBp2 and pPVX12D-GFP plasmids were digested with *Cla*I and *Spe*I restriction enzymes, gel purified, and then ligated (Fig. 1B).

The plasmids pRTL2-GFP, -GFP:TGBp1, -GFP:TGBp2, and -GFP:TGBp3 were prepared previously (Fig. 1; Yang et al., 2000; Krishnamurthy et al., 2003; Mitra et al., 2003). The pBIN-mGFP5-ER plasmid was obtained from Dr. J. Hasselof (Medical Research Council Laboratory of Molecular Biology, Cambridge, UK; Siemering et al., 1996); pDsRed-ST was a generous gift from Dr. R. Cyr (Pennsylvania State University, University Park, PA; Dixit and Cyr, 2002). pRTL2-GFP:Talin and -DsRed:Talin contain either enhanced GFP or DsRed (living colors; CLONTECH Laboratories, Palo Alto, CA) fused with the coding sequence of the F-actin-binding domain of mouse *Talin* (Kost et al., 1998; Fig. 1A).

BY-2 Protoplast Preparation and Transfection

Suspension cells of tobacco BY-2 (Nagata et al., 1992) were maintained as described in Qi and Ding (2002) with little change. BY-2 cells were propagated in the BY-2 culture medium (Murashige and Skoog medium [Murashige and Skoog salts; Sigma, St. Louis] supplemented with 30 g L^{-1} Suc, 256 mg L^{-1} KH_2PO_4, 100 mg L^{-1} myoinositol, 1 mg L^{-1} thiamine, and 0.2 mg L^{-1} 2,4-dichlorophenoxyacetic acid, pH 5.5 [w/v]) on a rotary shaker at 120 rpm at 28°C in the dark. Ten milliliters of BY-2 cells were transferred to 50 mL of fresh media weekly.

Protoplasts were isolated from the suspension cells as previously described with slight modifications (Gaire et al., 1999; Qi and Ding, 2002). Three-day-old cells in suspension culture media were collected by centrifugation at 200*g* for 5 min and resuspended in 1.5% cellulose Onozuka RS (w/v; Yakult Pharmaceutical, Tokyo) and 0.2% macerase (w/v; Calbiochem-Novabiochem, La Jolla, CA) in solution 1 [0.5 M mannitol, 3.6 mM MES, pH 5.5 (w/v)], and incubated for 3 to 5 h at 30°C in a water bath with a rotary shaker. The protoplasts were collected by filtration through 41-μm nylon mesh (Spectrum Laboratories, Rancho Dominguez, CA), and were centrifuged and washed twice with solution 1 at 100*g* for 5 min. Finally, protoplasts were resuspended in solution 2 (solution 1 plus 0.1 mM $CaCl_2$) to a density of about 2×10^6 protoplasts mL^{-1} and incubated on ice for 1 h.

Protoplasts were inoculated with infectious viral RNA transcripts. Transcripts were prepared from pPVX-GFP, pPVX12D-GFP, and pPVX-GFP:TGBp2 plasmids described previously (Baulcombe et al., 1995). Five micrograms of transcripts were used to transfect 5×10^5 BY-2 protoplasts. Electroporation was carried out at 0.25 kV, 100 Ω, and 125 μF using 0.4-cm gap cuvettes (Bio-Rad Laboratories, Hercules, CA) and a gene pulser (Bio-Rad Laboratories). Following electroporation, protoplasts were immediately transferred into a new tube containing 1 mL of solution 2 and incubated on ice for 30 min, and then at 30°C for 5 min. Protoplasts were collected by centrifugation at 39*g* for 5 min, resuspended in 1 mL of solution 3 (BY-2 culture media plus 0.45 M mannitol), and transferred to 6-well cell culture plates (Corning, Corning, NY) coated with solution 3 plus 1.0% agarose (w/v; pH 5.7). Protoplasts were cultured at 27°C and then collected at 18, 24, 36, and 48 hpi by centrifugation at 39*g* for 5 min.

Protoplasts were also transfected with pRTL2 plasmids by electroporation as described by Gaire et al. (1999) with a few changes. Protoplasts (1×10^6 in 0.5 mL) were mixed with 70 to 80 μg of plasmid DNA and 40 μg of sonicated salmon sperm DNA as carrier. The protoplast-DNA mixture was placed in a 0.4-cm gap cuvette (Bio-Rad Laboratories) on ice and then electroporated using a gene pulser (Bio-Rad Laboratories) at 0.18 kV, 100 Ω, and 125 μF with three pulses. Protoplasts were transferred after electroporation into a new tube containing 1 mL of solution 2, incubated on ice for 30 min, and then collected by centrifugation at 59*g* for 5 min. Protoplasts were resuspended in 1.5 mL of solution 3 (BY-2 culture media plus 0.45 M mannitol) and added to 6-well cell culture plates (Corning) containing solution 3 plus 1.0% agarose (w/v; pH 5.7). Protoplasts were cultured at 27°C for 18 h.

RNA- or DNA-transfected protoplasts were collected, washed with phosphate-buffered saline (PBS), and then fixed with PBS containing 3% paraformaldehyde (v/v) and 5 mM EGTA for 1 h at room temperature, followed by washing twice with PBS. Fixed samples were analyzed by confocal microscopy.

Some protoplasts were stained with DAPI. Transfected protoplasts were incubated in 10 μg mL^{-1} DAPI in growth media. Protoplasts were then analyzed by confocal microscopy.

Fluorometric Assays and Cycloheximide Treatment of BY-2 Protoplasts

In some experiments, protoplasts were inoculated with PVX transcripts or transfected with pRTL2 plasmids and fluorescence was monitored fluorometrically at 12, 18, 24, 30, 36, and 48 h as described previously (Howard et al., 2004). The average values from three samples were plotted at each time point. To measure protein turnover, solution 3 was removed at 24 hpt and replaced by solution 3 containing 500 μM cycloheximide (Sigma). Protoplasts were maintained in the 6-well cell culture plates at 27°C for an additional 4, 8, and 12 h. Nontreated protoplast samples were collected at 0 h (24 hpt) and immediately placed in liquid nitrogen. Cycloheximide-treated protoplasts were harvested by centrifugation at 59*g* for 5 min and immediately placed in liquid nitrogen. GFP expression was assayed by fluorometric analyses.

Plant Material and Plant Inoculations

Tobacco (*Nicotiana benthamiana* and *Nicotiana tabacum*) plants were used for studying the subcellular targeting of most proteins. Transgenic *N. tabacum* plants expressing mGFP5-ER, GFP:TGBp2, or GFP:TGBp3 were prepared previously using Agrobacterium transformation, as previously described (Krishnamurthy et al., 2003; Mitra et al., 2003).

Protoplasts were inoculated with PVX-GFP, PVX12D-GFP, and PVX-GFP:TGBp2 transcripts. Protoplasts were harvested and ground with an equal volume (w/v) of Tris-EDTA. Protoplast extracts were rub inoculated to *N. benthamiana* leaves with carborundum. Two leaves per plant were inoculated. Viruses spread systemically between 5 and 7 dpi. Leaves from systemically infected plants were harvested and used to inoculate further plants for microscopic analysis of virus infection. The leaf inoculum was prepared by grinding leaves 1:5 (w/v) in Tris-EDTA buffer. Two leaves per plant were each inoculated with 20-μL leaf extracts. Systemic spread of GFP expression was checked using a hand-held UV lamp.

Biolistic Bombardment

Tobacco (*N. benthamiana* and nontransgenic *N. tabacum*) source leaves were bombarded with pRTL2-GFP, -GFP:TGBp2, -GFP:TGBp3, -GFP:Talin, -DsRed:Talin, and pBIN-mGFP5-ER to study subcellular accumulation of the fusion proteins. Source leaves were identified by applying carboxyfluorescein dye (CF; Sigma) to the petiole of the most mature leaf of an *N. benthamiana* or tobacco plant (Yang et al., 2000; Krishnamurthy et al., 2002). Plants were kept in the dark overnight and the next day leaves were detached and observed using an epifluorescence microscope and a 10× objective lens. CF dye spread uniformly in sink leaves. CF dye resided only in the veins in source leaves. Following the CF dye experiments, source or sink leaves were detached from plants of similar age and bombarded with plasmids using the PDS 1000/He system (Bio-Rad Laboratories).

Leaves were bombarded with 10 μg plasmids mixed with 1 mg of 1-μm gold particles. Ten microliters of a DNA-gold mixture were loaded on a carrier disc and bombarded to detached leaves as described previously (Yang et al., 2000). The leaves were observed after 24 h using confocal microscopy.

Chemical Inhibitor Treatments of Leaves

Bombarded leaves were incubated overnight (16 h) on moist filter paper. Leaves were treated with either BFA, which disrupts the ER and Golgi network, or latrunculin B, which disrupts actin filaments (Henderson et al., 1994; Nebenfuhr et al., 1999; Ritzenthaler et al., 2002; Saint-Jore et al., 2002). Leaves were cut into segments, analyzed by epifluorescence microscopy to detect GFP expression, and then transferred to either a solution of 200 μg mL^{-1} BFA (Molecular Probes, Eugene, OR) or 1 μM latrunculin B (A.G. Scientific, San Diego). Each chemical inhibitor was dissolved in 0.1% DMSO (w/v) solution. Leaf segments were incubated in each chemical inhibitor solution for 2 to 4 h and then analyzed by confocal laser-scanning microscopy. As a control, leaf segments were incubated in sterile water or 0.1% DMSO (w/v) for 4 h and then analyzed by confocal laser-scanning microscopy.

Fixation, LR White Embedding, and Immunolabeling of Plant Material

For the electron microscopy studies, nontransgenic, mGFP5-ER, GFP:TGBp2, and GFP:TGBp3 transgenic tobacco leaf segments were fixed using the Balzer (Manchester, NH) HPM010 high-pressure freezing machine located at the Oklahoma Medical Research Center, according to standard protocols (Kiss et al., 1990). Leaf pieces were excised, washed with distilled, deionized water, and fitted into 0.4-mm freezer hats (Ted Pella, Reading, CA) filled with lecithin solution (100 mg mL^{-1} in chloroform). A drop of 15% (w/v) aqueous dextran (M_r 38,800) was added to each freezer hat. Freezer hats were then loaded onto a holder and inserted into the cryochamber at −80°C. Immediately after freezing, the freezer hats were transferred into Nalgene (Rochester, NY) cryogenic vials containing supercooled 100% acetone located in the liquid nitrogen bath.

Freeze substitution was carried out by transferring samples from the freezer hats to a solution of 1% OsO_4 and acetone. Samples were maintained in a dry ice/acetone bath for 2.5 d at −78.6°C. Samples were transferred from the freezer hats to vials of acetone and incubated in a freezer at −20°C for 2 h, then in a refrigerator at 0°C for 2 h, and then on the lab bench (23°C) for 2 h. Samples in vials were then rinsed three times in acetone for 20 min, three times in 100% ethanol for 20 min, and then embedded in LR White resin.

Ultrathin sections (60 nm) were cut using a diamond knife on a Sorvall MT 6000 ultramicrotome and mounted on formvar-coated nickel grids (Electron Microscopy Science, Hatfield, PA). Immunogold labeling of LR White-embedded tissues was conducted using full-length mouse monoclonal AV antisera (BD living colors; CLONTECH Laboratories) to detect GFP and rabbit polyclonal BiP antisera obtained from Dr. R. Boston (North Carolina State University). Grids were incubated in blocking solution consisting of PBS, pH 7.5 (130 mM NaCl, 7.0 mM Na_2HPO_4, 3.0 mM NaH_2PO_4) plus 2% bovine serum albumin (BSA; w/v) for 15 min, and then incubated with 2% normal goat serum (obtained from Astri Wayandande, Oklahoma State University) in PBS plus 2% BSA for 15 min. Then samples were incubated with either anti-GFP sera diluted 1:500 in PBS plus 2% BSA (w/v), or BiP antisera diluted 1:10 in PBS plus 0.1% Tween (v/v), or buffer containing no primary antisera for 2 h. The grids were then washed five times for 5 min with PBS and then with PBS plus 2% fish gelatin (v/v) for 15 min. The grids were then incubated for 1 h with either 10 or 25 nm gold-conjugated rabbit antisera (EY Labs, San Mateo, CA) diluted 1:10 in PBS plus 2% fish gelatin. Grids were washed three times for 5 min with distilled, deionized water, and stained with a solution of 2.5% uranyl acetate and 70% methanol (v/v) for 30 min, and then with a solution of 2% Reynold's lead citrate, pH 12.0 (in distilled, deionized water) for 20 min. Samples were washed with lukewarm distilled, deionized water three times for 5 min and then dried. Control samples were incubated with either blocking solution only or blocking solution plus 10 nm gold-conjugated rabbit antisera.

For dual labeling to detect BiP and GFP or TMV and GFP, a longer procedure was followed. Samples were first incubated with BiP or TMV antiserum diluted 1:10 or 1:50, respectively, in PBS plus 0.1% Tween (v/v) for 2 h and then with the 25-nm gold-conjugated rabbit antisera diluted 1:10 in PBS plus 2% fish gelatin for 2 h as described above. Samples were washed twice for 10 min with PBS and then incubated for 30 min with full-length mouse monoclonal AV antisera diluted 1:500 in PBS. Samples were washed five times for 5 min with PBS, then for 15 min with PBS with 2% fish gelatin, and then incubated with for 30 min with 10 nm gold-conjugated secondary antibody (EY Labs) diluted 1:10 in PBS plus 2% fish gelatin. Grids were washed twice for 10 min with PBS, three times for 5 min with distilled, deionized water. Samples were stained with uranyl acetate and Reynold's lead citrate as described above.

Confocal and Electron Microscopy

A Leica TCS SP2 (Leica Microsystems, Bannockburn, IL) or a Bio-Rad 1024ES (Bio-Rad Laboratories) confocal imaging system was used to study subcellular localization of the GFP fusion proteins in tobacco epidermal cells that were either bombarded with plasmids or inoculated with the PVX viruses. The Leica TCS SP2 system was attached to a Leica DMRE microscope. The Bio-Rad 1024ES system was attached to a Zeiss Axioskop (Carl Zeiss, Thornwood, NY) and was used for experiments involving GFP:Talin and DsRed:Talin. Both microscopes were equipped with epifluorescence and water immersion objectives. For confocal microscopy, a UV laser and a krypton/argon laser were used to examine fluorescence. A 488-nm excitation wavelength was used to view GFP expression, a 358-nm excitation wavelength was used to view DAPI, and 543- or 568-nm excitation wavelengths were used to examine DsRed expression. In general, 15 to 30 optical sections were taken of each cell at 0.3- to 2-μm intervals.

Electron microscopic analysis of samples was carried out using a JEOL JEM 100 CXII scanning transmission electron microscope. Photographs were taken and developed in a dark room and then scanned using an HP scan jet 4570c. All images obtained by epifluorescence, confocal, or electron microscopy were processed using Adobe Photoshop CS version 8.0 software (Adobe Systems, San Jose, CA).

Statistical Analyses

Logistic regression for fluorescence in each subcellular address (vesicle, nucleus, and cytoplasm), with the presence/absence of each address as the response variable and time as the independent variable was performed using data presented in Figure 1, J and K (PROC LOGISTIC, PC SAS, version 8.2; SAS Institute, Cary, NC). These regressions were performed for both the PVX-GFP:TGBp2 and PVX-GFP. Slope estimates and P values were determined.

Linear and polynomial regressions were used to find the best-fit curve for comparing fluorescence in BY-2 protoplasts before and after cycloheximide treatments in Figure 4. The distribution fluorescence in BY-2 protoplasts recorded in Table I was analyzed with pairwise Fisher's exact tests using PROC FREQ in PC SAS version 8.2. A significance level of 0.05 was used for all comparisons.

ANOVA procedures with PC SAS version 8.2 (SAS Institute) and PROC GLM were used to evaluate differences in location in the number of gold particles observed in the electron micrographs that were reported in Table II. The analysis was performed for each combination of transgene and antiserum. Due to problems in homogeneity of variance and distributional assumptions, a square-root transformation was used prior to conducting the ANOVAs. When the ANOVA was significant, pairwise comparisons of the locations were made with a PDIFF option in an LSMEANS statement. A significance level of 0.05 was used for all comparisons.

Upon request, all novel materials described in this publication will be made available in a timely manner for noncommercial research purposes, subject to the requisite permission from any third-party owners of all or parts of the material. Obtaining permission will be the responsibility of the requester.

ACKNOWLEDGMENTS

We would like to thank Phoebe Doss and Terry Colburn at the Oklahoma State University Electron Microscopy Center and Ben Fowler at Oklahoma Medical Research Foundation (OMRF) for assistance with cryofixation microscopy. Further appreciation is extended to Barbara Driskel for greenhouse support and to Dr. Biao Ding (Ohio State University) for technical advice and useful discussions.

Received May 23, 2005; revised June 8, 2005; accepted June 8, 2005; published July 29, 2005.

LITERATURE CITED

Allison A, Shalla T (1973) The ultrastructure of local lesions induced by *Potato virus X*: a sequence of cytological events in the course of infection. Phytopathology **64:** 784–793

Baluska F, Samaj J, Napier R, Volkmann D (1999) Maize calreticulin localizes preferentially to plasmodesmata in root apex. Plant J **19:** 481–488

Baulcombe DC, Chapman S, Santa Cruz S (1995) Jellyfish green fluorescent protein as a reporter for virus infections. Plant J **7:** 1045–1053

Boevink P, Oparka K, Santa Cruz S, Martin B, Betteridge A, Hawes C (1998) Stacks on tracks: the plant Golgi apparatus traffics on an actin/ER network. Plant J **15:** 441–447

Brandizzi F, Hanton S, DaSilva LL, Boevink P, Evans D, Oparka K, Denecke J, Hawes C (2003) ER quality control can lead to retrograde transport from the ER lumen to the cytosol and the nucleoplasm in plants. Plant J **34:** 269–281

Brandizzi F, Snapp EL, Roberts AG, Lippincott-Schwartz J, Hawes C (2002) Membrane protein transport between the endoplasmic reticulum

and the Golgi in tobacco leaves is energy dependent but cytoskeleton independent: evidence from selective photo bleaching. Plant Cell **14:** 1293–1309

Brigneti G, Voinnet O, Li WX, Ji LH, Ding SW, Baulcombe DC (1998) Viral pathogenicity determinants are suppressors of transgene silencing in *Nicotiana benthamiana*. EMBO J **17:** 6739–6746

Carette JE, Guhl K, Wellink J, Van Kammen A (2002a) Coalescence of the sites of *Cowpea mosaic virus* RNA replication into a cytopathic structure. J Virol **76:** 6235–6243

Carette JE, van Lent J, MacFarlane SA, Wellink J, van Kammen A (2002b) *Cowpea mosaic virus* 32- and 60-kilodalton replication proteins target and change the morphology of endoplasmic reticulum membranes. J Virol **76:** 6293–6301

Cowan GH, Lioliopoulou F, Ziegler A, Torrance L (2002) Subcellular localisation, protein interactions, and RNA binding of Potato mop-top virus triple gene block proteins. Virology **298:** 106–115

Crawford KM, Zambryski PC (2000) Subcellular localization determines the availability of non-targeted proteins to plasmodesmatal transport. Curr Biol **10:** 1032–1040

Crawford KM, Zambryski PC (2001) Non-targeted and targeted protein movement through plasmodesmata in leaves in different developmental and physiological states. Plant Physiol **125:** 1802–1812

Di Cola A, Frigerio L, Lord JM, Ceriotti A, Roberts LM (2001) Ricin A chain without its partner B chain is degraded after retrotranslocation from the endoplasmic reticulum to the cytosol in plant cells. Proc Natl Acad Sci USA **98:** 14726–14731

Ding XS, Liu J, Cheng NH, Folimonov A, Hou YM, Bao Y, Katagi C, Carter SA, Nelson RS (2004) The *Tobacco mosaic virus* 126-kDa protein associated with virus replication and movement suppresses RNA silencing. Mol Plant Microbe Interact **17:** 583–592

Dixit R, Cyr R (2002) Golgi secretion is not required for marking the preprophase band site in cultured tobacco cells. Plant J **29:** 99–108

Drugeon G, Jupin I (2002) Stability in vitro of the 69K movement protein of *Turnip yellow mosaic virus* is regulated by the ubiquitin-mediated proteasome pathway. J Gen Virol **83:** 3187–3197

Dunoyer P, Ritzenthaler C, Hemmer O, Michler P, Fritsch C (2002) Intracellular localization of the *Peanut clump virus* replication complex in tobacco BY-2 protoplasts containing green fluorescent protein-labeled endoplasmic reticulum or Golgi apparatus. J Virol **76:** 865–874

Erhardt M, Morant M, Ritzenthaler C, Stussi-Garaud C, Guilley H, Richards K, Jonard G, Bouzoubaa S, Gilmer D (2000) P42 movement protein of *Beet necrotic yellow vein virus* is targeted by the movement proteins P13 and P15 to punctate bodies associated with plasmodesmata. Mol Plant Microbe Interact **13:** 520–528

Espinoza AM, Medina V, Hull R, Markham PG (1991) *Cauliflower mosaic virus* gene II product forms distinct inclusion bodies in infected plant cells. Virology **185:** 337–344

Fontes EB, Shank BB, Wrobel RL, Moose SP, OBrian GR, Wurtzel ET, Boston RS (1991) Characterization of an immunoglobulin binding protein homolog in the maize floury-2 endosperm mutant. Plant Cell **3:** 483–496

Gaire F, Schmitt C, Stussi-Garaud C, Pinck L, Ritzenthaler C (1999) Protein 2A of grapevine fanleaf nepovirus is implicated in RNA2 replication and colocalizes to the replication site. Virology **264:** 25–36

Gillespie T, Boevink P, Haupt S, Roberts AG, Toth R, Valentine T, Chapman S, Oparka KJ (2002) Functional analysis of a DNA-shuffled movement protein reveals that microtubules are dispensable for the cell-to-cell movement of *Tobacco mosaic virus*. Plant Cell **14:** 1207–1222

Gorshkova EN, Erokhina TN, Stroganova TA, Yelina NE, Zamyatnin AA Jr, Kalinina NO, Schiemann J, Solovyev AG, Morozov SY (2003) Immunodetection and fluorescent microscopy of transgenically expressed hordeivirus TGBp3 movement protein reveals its association with endoplasmic reticulum elements in close proximity to plasmodesmata. J Gen Virol **84:** 985–994

Haupt S, Cowan GH, Ziegler A, Roberts AB, Oparka KJ, Torrance L (2005) Two plant-viral movement proteins traffic in the endocytic recycling pathway. Plant Cell **17:** 164–181

Heinlein M, Epel BL, Padgett HS, Beachy RN (1995) Interaction of tobamovirus movement proteins with the plant cytoskeleton. Science **270:** 1983–1985

Heinlein M, Padgett HS, Gens JS, Pickard BG, Casper SJ, Epel BL, Beachy RN (1998) Changing patterns of localization of the *Tobacco mosaic virus* movement protein and replicase to the endoplasmic reticulum and microtubules during infection. Plant Cell **10:** 1107–1120

Henderson J, Satiat-Jeunemaitre B, Napier R, Hawes C (1994) Brefeldin A-induced disassembly of the Golgi apparatus is followed by disruption of the endoplasmic reticulum in plant cells. J Exp Bot **45:** 1347–1351

Howard AR, Heppler ML, Ju H-J, Krishnamurthy K, Payton ME, Verchot-Lubicz J (2004) *Potato virus X* TGBp1 induces plasmodesmata gating and moves between cells in several host species whereas CP moves only in *N. benthamiana* leaves. Virology **328:** 185–197

Huisman MJ, Linthorst HJ, Bol JF, Cornelissen JC (1988) The complete nucleotide sequence of *Potato virus X* and its homologies at the amino acid level with various plus-stranded RNA viruses. J Gen Virol **69:** 1789–1798

Kawakami S, Watanabe Y, Beachy RN (2004) *Tobacco mosaic virus* infection spreads cell to cell as intact replication complexes. Proc Natl Acad Sci USA **101:** 6291–6296

Kikumoto T, Matsui C (1961) Electron microscopy of intracellular *Potato virus X*. Virology **13:** 294–299

Kirst ME, Meyer DJ, Gibbon BC, Jung R, Boston RS (2005) Identification and characterization of endoplasmic reticulum-associated degradation proteins differentially affected by endoplasmic reticulum stress. Plant Physiol **138:** 218–231

Kiss JZ, Giddings TH Jr, Staehelin LA, Sack FD (1990) Comparison of the ultrastructure of conventionally fixed and high pressure frozen/freeze substituted root tips of *Nicotiana* and *Arabidopsis*. Protoplasma **157:** 64–74

Knebel W, Quader H, Schnepf E (1990) Mobile and immobile endoplasmic reticulum in onion bulb epidermis cells: short- and long-term observations with a confocal laser scanning microscope. Eur J Cell Biol **52:** 328–340

Kost B, Spielhofer P, Chua N-H (1998) A GFP-mouse talin fusion protein labels plant actin filaments in vivo and visualizes the actin cytoskeleton in growing pollen tubes. Plant J **16:** 393–401

Kozar FE, Sheludko YM (1969) Ultrastructure of potato and *Datura stramonium* plant cells infected with *Potato virus X*. Virology **38:** 220–229

Krishnamurthy K, Heppler M, Mitra R, Blancaflor E, Payton M, Nelson RS, Verchot-Lubicz J (2003) The potato virus X TGBp3 protein associates with the ER network for virus cell-to-cell movement. Virology **309:** 135–151

Krishnamurthy K, Mitra R, Payton ME, Verchot-Lubicz J (2002) Cell-to-cell movement of the PVX 12K, 8K, or coat proteins may depend on the host, leaf developmental stage, and the PVX 25K protein. Virology **300:** 269–281

Lee WM, Ahlquist P (2003) Membrane synthesis, specific lipid requirements, and localized lipid composition changes associated with a positive-strand RNA virus RNA replication protein. J Virol **77:** 12819–12828

Liu J-Z, Blancaflor EB, Nelson RS (2005) The tobacco mosaic virus 126-kilodalton protein, a constituent of the virus replication complex, alone or within the complex aligns with and traffics along microfilaments. Plant Physiol **138:** 1853–1865

Martinez IM, Chrispeels MJ (2003) Genomic analysis of the unfolded protein response in Arabidopsis shows its connection to important cellular processes. Plant Cell **15:** 561–576

Mas P, Beachy RN (1999) Replication of *Tobacco mosaic virus* on endoplasmic reticulum and role of the cytoskeleton and virus movement protein in intracellular distribution of viral RNA. J Cell Biol **147:** 945–958

McCann RO, Craig SW (1997) The I/LWEQ module: a conserved sequence that signifies F-actin binding in functionally diverse proteins from yeast to mammals. Proc Natl Acad Sci USA **94:** 5679–5684

McLean BG, Zupan J, Zambryski PC (1995) *Tobacco mosaic virus* movement protein associates with the cytoskeleton in tobacco cells. Plant Cell **7:** 2101–2114

Mitra R, Krishnamurthy K, Blancaflor E, Payton M, Nelson RS, Verchot-Lubicz J (2003) The *Potato virus X* TGBp2 protein association with the endoplasmic reticulum plays a role in but is not sufficient for viral cell-to-cell movement. Virology **312:** 35–48

Morozov SY, Solovyev AG (2003) Triple gene block: modular design of a multifunctional machine for plant virus movement. J Gen Virol **84:** 1351–1366

Nagata T, Nemoto Y, Hasezawa S (1992) Tobacco BY-2 cell line as the ''Hela'' cell in the cell biology of higher plants. Int Rev Cytol **132:** 1–31

Navazio L, Mariani P, Sanders D (2001) Mobilization of Ca^{2+} by cyclic

ADP-ribose from the endoplasmic reticulum of cauliflower florets. Plant Physiol **125:** 2129–2138

Nebenfuhr A, Gallagher L, Dunahay T, Frohlick J, Mazurkiewicz A, Meehl J, Staehelin LA (1999) Stop-and-go movements of plant Golgi stacks are mediated by the acto-myosin system. Plant Physiol **121:** 1127–1142

Nebenfuhr A, Ritzenthaler C, Robinson DG (2002) Brefeldin A: deciphering an enigmatic inhibitor of secretion. Plant Physiol **130:** 1102–1108

Nelson RS (2005) Movement of viruses to and through plasmodesmata. *In* K Oparka, ed, Plasmodesmata. Blackwell Publishing Ltd, Oxford, pp 188–209

Oparka KJ, Roberts AG, Boevink P, Santa Cruz S, Roberts I, Pradel KS, Imlau A, Kotlizky G, Sauer N, Epel B (1999) Simple, but not branched, plasmodesmata allow the nonspecific trafficking of proteins in developing tobacco leaves. Cell **97:** 743–754

Qi Y, Ding B (2002) Replication of *Potato spindle tuber viroid* in cultured cells of tobacco and *Nicotiana benthamiana*: the role of specific nucleotides in determining replication levels for host adaptation. Virology **302:** 445–456

Reichel C, Beachy RN (1998) *Tobacco mosaic virus* infection induces severe morphological changes of the endoplasmic reticulum. Proc Natl Acad Sci USA **95:** 11169–11174

Reichel C, Beachy RN (2000) Degradation of *Tobacco mosaic virus* movement protein by the 26S proteasome. J Virol **74:** 3330–3337

Reichelt S, Knight AE, Hodge TP, Baluska F, Samaj J, Volkmann D, Kendrick-Jones J (1999) Characterization of the unconventional myosin VIII in plant cells and its localization at the post-cytokinetic cell wall. Plant J **19:** 555–567

Ritzenthaler C, Laporte C, Gaire F, Dunoyer P, Schmitt C, Duval S, Piequet A, Loudes AM, Rohfritsch O, Stussi-Garaud C, et al (2002) *Grapevine fanleaf virus* replication occurs on endoplasmic reticulum-derived membranes. J Virol **76:** 8808–8819

Rouleau M, Smith RJ, Bancroft JB, Mackie GA (1994) Purification, properties, and subcellular localization of foxtail mosaic potexvirus 26-kDa protein. Virology **204:** 254–265

Rubino L, Russo M (1998) Membrane targeting sequences in tombusvirus infections. Virology **252:** 431–437

Rubino L, Weber-Lotfi F, Dietrich A, Stussi-Garaud C, Russo M (2001) The open reading frame 1-encoded ('36K') protein of *Carnation Italian ringspot virus* localizes to mitochondria. J Gen Virol **82:** 29–34

Saint-Jore C, Evins J, Batoko H, Brandizzi F, Moore I, Hawes C (2002) Redistribution of membrane proteins between the Golgi apparatus and endoplasmic reticulum in plants is reversible and not dependent on cytoskeletal networks. Plant J **29:** 661–678

Sambrook J, Fritsch EF, Maniatis T (1989) Molecular Cloning: A Laboratory Manual, Ed 2. Cold Spring Harbor Laboratory Press, Cold Spring Harbor, NY

Schaad MC, Jensen PE, Carrington JC (1997) Formation of plant RNA virus replication complexes on membranes: role of an endoplasmic reticulum-targeted viral protein. EMBO J **16:** 4049–4059

Schwartz M, Chen J, Janda M, Sullivan M, den Boon J, Ahlquist P (2002) A positive-strand RNA virus replication complex parallels form and function of retrovirus capsids. Mol Cell **9:** 505–514

Schwartz M, Chen J, Lee WM, Janda M, Ahlquist P (2004) Alternate, virus-induced membrane rearrangements support positive-strand RNA virus genome replication. Proc Natl Acad Sci USA **101:** 11263–11268

Siemering K, Golbik R, Sever R, Haseloff J (1996) Mutations that suppress the thermosensitivity of green fluorescent protein. Curr Biol **6:** 1653–1663

Smalle J, Vierstra RD (2004) The ubiquitin 26S proteasome proteolytic pathway. Annu Rev Plant Biol **55:** 555–590

Solovyev AG, Stroganova TA, Zamyatnin AA Jr, Fedorkin ON, Schiemann J, Morozov SY (2000) Subcellular sorting of small membrane-associated triple gene block proteins: TGBp3-assisted targeting of TGBp2. Virology **269:** 113–127

Spillane C, Verchot J, Kavanagh TA, Baulcombe DC (1997) Concurrent suppression of virus replication and rescue of movement-defective virus in transgenic plants expressing the coat protein of *Potato virus X*. Virology **236:** 76–84

Szecsi J, Ding XS, Lim CO, Bendahmane M, Cho MJ, Nelson RS, Beachy RN (1999) Development of *Tobacco mosaic virus* infection sites in *Nicotiana benthamiana*. Mol Plant Microbe Interact **12:** 143–152

Turner KA, Sit TL, Callaway AS, Allen NS, Lommel SA (2004) *Red clover necrotic mosaic virus* replication proteins accumulate at the endoplasmic reticulum. Virology **320:** 276–290

Verchot J, Angell SM, Baulcombe DC (1998) In vivo translation of the triple gene block of *Potato virus X* requires two subgenomic mRNAs. J Virol **72:** 8316–8320

Verchot-Lubicz J (2005) A new model for cell-to-cell movement of potexviruses. Mol Plant Microbe Interact **18:** 283–290

Yang Y, Ding B, Baulcombe DC, Verchot J (2000) Cell-to-cell movement of the 25K protein of *Potato virus X* is regulated by three other viral proteins. Mol Plant Microbe Interact **13:** 599–605

Zamyatnin AA Jr, Solovyev AG, Savenkov EI, Germundsson A, Sandgren M, Valkonen JP, Morozov SY (2004) Transient coexpression of individual genes encoded by the triple gene block of *Potato mop-top virus* reveals requirements for TGBp1 trafficking. Mol Plant Microbe Interact **17:** 921–930